KING'S College LONDON
University of London

Division of Engineering
Department of Mechanical Engineering

AUTOMATED EXCAVATION

Kasambula Vincent de Paul

Project supervisors: Dr. Kaspar Althoefer, Prof. Lakmal Seneviratne

A Dissertation submitted to the King's College London
In Partial Fulfilment of the Requirement for
Master of Science in Mechatronics

12th September 2003

This report, submitted to the Department of Mechanical Engineering, King's College London, is solely an original work of its author, except where clearly specified otherwise. It has not been previously submitted to this or another University.

Kasambula Vincent de Paul

Dedicated to Arnold and Priscilla

Acknowledgments

I would like to thank my project supervisor Dr. Kaspar Althoefer whose guidance enabled me accomplish this piece of work. Special thanks go to my second supervisor Prof. Lakmal Seneviratne (who is also the course director) for his encouragement. Thanks to PhD student Choopar Tan for assistance with the experiments and last but not least special thanks to Darrell and Denise Kawooya's family for their unreserved support.

Abstract

In this project soil-tool interaction forces during excavation were examined. To do this a test-rig was developed and used to record and compute magnitudes of soil failure forces obtained from experimenting on three types of soil. A flat blade assembly fitted with a force-torque sensor and gripped by a robotic hand was used to execute excavation in a laboratory-size soil bed also developed by this project. The robotic hand was programmed to facilitate experimentation with different settings of blade insertion angles and insertion depths. The computed soil failure forces were in turn used to estimate soil properties using a soil property estimation technique being developed at the College. Project tasks included design and construction of the said test rig, incorporating into it a Force-Torque sensing scheme for quantifying forces imparted to the excavation blade, programming a robot arm to carry out robotic excavation, setting up a system for collecting and processing of the force-torque data and finally use of the analysed data to estimate properties of the soil samples. If sources of errors are eliminated, the experimental methods developed can helpful to the development of on line soil property estimation for excavation machines.

Contents

List of figures

1 Introduction and Background

Industries in which earthmoving plays a fundamental role are constantly under pressure to improve their productivity in terms of amount of work accomplished from limited inputs, efficiency in terms of optimal labour and machinery costs, as well as safety in terms of minimised injury to workers. Traditional means of improving excavation have been to make excavation mechanisms more efficient through progressive increases in size and power. Practical limits have been reached and now, given that it greatly improves machine and human operator performance, automation of excavation tasks is increasingly being seen as the way forward. Apart from needs driven by economic concerns, automated excavation is also motivated by health concerns in worksites (like war zones, waste disposal sites, etc) that are hazardous to humans. Since field worthy earthmovers must often operate in unstructured and dynamic environments, realizing their automation is an intricate task. Nevertheless, advances in computing and sensory technologies, which have fast, compact and rugged components provide incentive to overcome the obstacles.

In reality most seemingly automated systems are partially automated as opposed to being fully autonomous. At some stage within the cycle, human input or control must intervene to achieve some function. At one extreme are tele-operated systems, which depend on a human operator for every motion, while at the other extreme are systems that are initially imparted with intelligence to sense, plan, and act autonomously.

Enabling technologies used to automate excavation systems are ***sensing*** of the machines' state and the environments in which they operate, ***modular designs*** of machine implements for effective interaction with the earth and ***soil-tool interaction models*** that outline soil properties. [2]. By providing optimized digging trajectories for a given excavation task, online soil property estimation contributes to development of excavation strategies for autonomous excavator vehicles. [1]. Further more; soil properties of major interest to excavation activities are those parameters that constitute the soil's physical strength. By examining soil tool interactive forces, it must therefore be possible to get reasonable measures of physical properties for a given soil. This project considered automated excavation at the level where soil-tool interaction related to forces involved during excavation.

1.1 Project Scope

The project focused on experimental micro-robotic interactions between a soil and an excavation tool whereby possible resultant forces acting on the tool, as a result of a combination of robotic forces and internal resistive soil forces, were developed and used to compute soil failure forces. A test rig, comprising of a Mitsubishi RV-M1 Robot arm, a soil bed, a Force-Torque sensor, a data acquisition system and a personal computer, was developed. The project scope was the use of micro-robotic excavation to carry out controlled soil tool interaction so that forces involved as the tool interacted with the soil were detected, recorded and processed.

1.2 Aims and objectives

The aim was to acquire and process soil-tool interaction forces based on five different blade insertion angles and two different blade insertion depths. To this end, experiments were formulated and conducted on three different cohesion-less soils based on measurably adjustable quantities within the test-rig. The other objective was to estimate soil parameters from soil failure forces that were computed using detected forces and geometrical structure of the excavation blade. To this end, one soil parameter estimation technique being developed by [1] was tried out with experimental data obtained from the test rig.

1.3 Theoretical development

In order to understand how soil properties relate to soil failure force, it necessary to study various soil models in existence. Although they are all not necessarily in agreement they provide a theoretical basis on which experiments and experimental results analyses are carried out. Here soil modelling is used as a means of predicting the force required to move a flat plate embedded in a soil medium.

1.3.1 The Mohr-Coulomb failure law

As adapted from [3] the Mohr-Coulomb failure law provides an expression for shear strength of soil s as:

$$s = c + \sigma \tan \phi \qquad (1)$$

where s = shearing resistance of he soil
c = soil cohesion
σ = Normal stress applied on the shear surface
ϕ = angle of shearing resistance

There is therefore a similar computation for soil shear along a soil-tool interface. For cohesion-less soils where **c** = 0, the relationship between the angle of shearing resistance, ϕ and the coefficient of friction, μ is

$$\mu = \tan \phi \quad \Rightarrow \quad \phi = \tan^{-1} \mu \quad = \tan^{-1} \left[\frac{s}{\sigma} \right] \qquad (2)$$

This equation was used in conjunction with experimental data to estimate soil tool interface friction angle as is seen in section 3.2.

1.4 Soil Modelling (adapted from [3])

For the plate to move, soil must be displaced. This occurs with a failure surface developing between the moving soil in the immediate vicinity of the blade and the stationary soil beyond the vicinity of the blade. The strength of a soil interprets into stress conditions that lead to soil failure. This can be matched to the classical Mohr-Coulomb soil model of passive and active pressure [Coulomb, 1776] and to the Chen and Liu Upper Bound (CLUB) soil model associated with the velocity condition and energy dissipation of the soil [Chen-Liu, 1990]. The former provided the platform for developing and carrying out experiments as well as a theoretical basis for analysis of the obtained experimental results.

1.4.1 Mohr-Coulomb soil model (adapted from [3])

This model characterises soil strength as a combination of internal friction and cohesion. It is two-dimensional and uses parameters of soil-soil friction ϕ, soil-tool friction δ, soil density γ, tool depth H, and tool orientation α to predict resistive forces on a tool moving through the terrain. Forces required to accelerate the soil are ignored and it is assumed a planar failure surface occurs between the moving soil in the immediate vicinity of the blade and the stationary soil beyond the vicinity of the blade. The soil is assumed to be homogeneous so that perfect plastic deformation is supposed to occur. Assuming static equilibrium and that the shape of the failure surface approximated by a unit width plane, as shown in figure 1, three main forces acting on wedge ABC are weight of the wedge **W**, soil-soil friction force **F** and soil-tool interface friction force $\mathbf{P_P}$

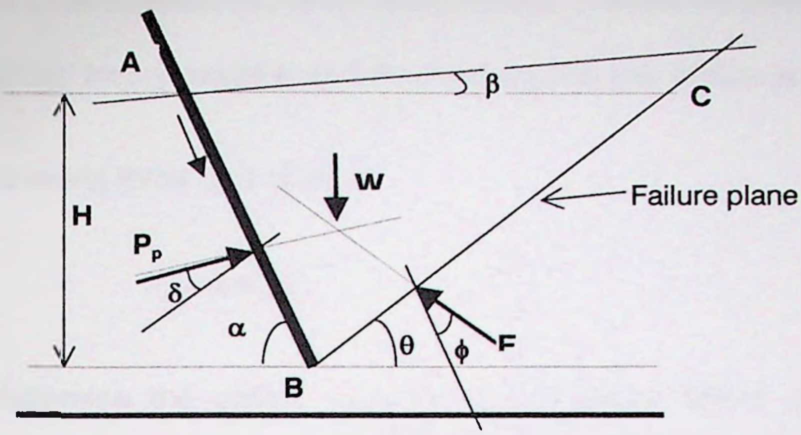

FIGURE 1. STATIC EQUILIBRIUM ANALYSIS OF A FLAT BLADE MOVING THROUGH SOIL. It assumes that a planar failure surface forms a triangular wedge ABC when the blade moves forward.

If **W** is known both in magnitude and direction, the magnitude of **F** and $\mathbf{P_P}$ can be obtained by applying a force equilibrium analysis on the wedge. However this analysis does not provide any information on their line of action towards the tool and the failure plane.

The model computes the failure force based on the idea of active earth pressure and passive earth pressure, which are the soil pressure applied to the back of the blade and the pressure required to fail the soil in the front of the blade, respectively.

The failure force **F** is computed as, Passive force $\mathbf{F_P}$ minus Active force $\mathbf{F_A}$ as depicted in equation(3),

$$F = F_P - F_A = \frac{1}{2}\gamma H^2\left(K_P(\alpha,\beta,\phi,\delta) - K_A(\alpha,\beta,\phi,\delta)\right) \tag{3}$$

Where, γ is soil density, **H** is vertical insertion depth of blade, $\mathbf{K_P}$ and $\mathbf{K_A}$ are passive and active force coefficients, which are functions of blade insertion angle α, soil surface angle β, soil-soil friction angle ϕ, and the interface soil-tool friction angle δ.

The drawing force $\mathbf{F_P}$ is given as

$$F_P = \min\left|P_P\right| \tag{4}$$

To determine the critical value of θ, the planar failure plane problem is examined graphically and analytically and the force $\mathbf{P_P}$ is expressed as a function of and differentiated with respect to θ.

Substituting the critical value into the original equation gives an expression for $\mathbf{F_P}$

$$F_P = \frac{1}{2}\gamma H^2 \frac{K_P}{\sin\alpha\cos\delta} \tag{5}$$

Where $\mathbf{K_P}$ is given as

$$K_P = \frac{\sin^2(\alpha-\phi)\cos\delta}{\sin\alpha\sin(\alpha+\delta)\left\{1-\sqrt{\dfrac{\sin(\phi+\delta)\sin(\phi+\beta)}{\sin(\alpha+\delta)\sin(\alpha+\beta)}}\right\}^2} \tag{6}$$

A similar derivation is repeated for the active earth pressure and an expression for $\mathbf{F_A}$ obtained.

$$F_A = \frac{1}{2}\gamma H^2 \frac{K_A}{\sin\alpha_A \cos\delta} \quad (7)$$

Where $\mathbf{K_A}$ is given as

$$K_A = \frac{\sin^2(\alpha_A + \phi)\cos\delta}{\sin\alpha_A \sin(\alpha_A - \delta)\left\{1 - \sqrt{\frac{\sin(\phi+\delta)\sin(\phi-\beta_A)}{\sin(\alpha_A-\delta)\sin(\alpha_A+\beta_A)}}\right\}^2} \quad (8)$$

With $\alpha_A = \pi - \alpha \quad and \quad \beta_A = -\beta$

The failure force **F** is obtained by substituting equations (6) and (8) into (3),

1.4.2 **Chen and Liu Upper Bound (CLUB) soil mode** (adapted from [3])

The equation derived from the CLUB model is associated with the velocity condition and energy dissipation of the soil. The failure mechanism is divided into three regions as shown in Figure 2.

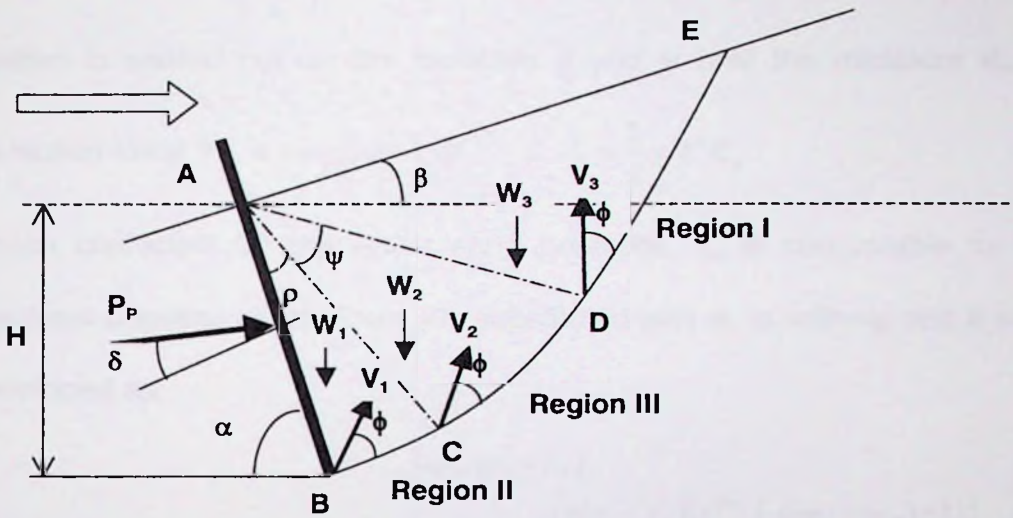

FIGURE 2. THE CLUB SOIL MODEL

It assumes a curved failure region ACD when the blade is pushed forward.

Region **I** is a triangular region assumed not to be affected by the soil tool interface friction. Region **II** also has a triangular section but the interface friction influences it. Region **III** is a transition zone with a logarithmic spiral pattern. Based on the three-region mechanism and the energy dissipation analysis, Chen and Liu developed an upper bound for the coefficient of passive earth pressure $\mathbf{K_p}$ as,

$$K_p = \frac{c(\rho_f - \phi)s\alpha}{s^2\alpha c\phi\left(s(\alpha+\delta)c\rho_f - c\delta t\delta c(\alpha - \rho_f)\right)} \left\{ \begin{array}{l} s\rho_f c(\alpha - \rho_f) \\ + \dfrac{c(\rho_f - \phi)}{(b^2+1)c\phi} \left[\begin{array}{l} c(\alpha - \rho_f)\left(e^{b\psi_f}(bc\psi_f + s\psi_f) - b\right) \\ + s(\alpha - \rho_f)\left(e^{b\psi_f}(bs\psi_f - c\psi_f) + 1\right) \end{array} \right] \\ + \dfrac{c(\rho_f - \phi)s(\alpha + \beta - \rho_f - \psi_f)c(\alpha - \rho_f - \psi_f)e^{b\psi_f}}{c(\alpha + \beta + \phi - \rho_f - \psi_f)} \end{array} \right\} \quad (9)$$

Optimisation is carried out on the variables ρ and ψ until the minimum $\mathbf{K_p}$ is found.

Passive friction force, $\mathbf{F_P}$, is computed as $F_P = \frac{1}{2}\gamma H^2 K_p$

The friction coefficient for the active earth pressure, $\mathbf{K_A}$ is comparable to $\mathbf{K_P}$ except variables have opposite signs. Thus, ϕ is substituted with $-\phi$, ψ_f with $-\psi_f$ and **b** with **–b** and $\mathbf{K_A}$ is developed as;

$$K_A = \frac{c(\rho_f + \phi)s\alpha_A}{s^2\alpha_A c\phi\left(s(\alpha_A+\delta)c\rho_f - c\delta t\delta c(\alpha_A - \rho_f)\right)} \left\{ \begin{array}{l} s\rho_f c(\alpha_A - \rho_f) \\ + \dfrac{c(\rho_f + \phi)}{(b^2+1)c\phi} \left[\begin{array}{l} c(\alpha_A - \rho_f)\left(e^{-b\psi_f}(-bc\psi_f + s\psi_f) + b\right) \\ - s(\alpha_A - \rho_f)\left(e^{-b\psi_f}(bs\psi_f + c\psi_f) + 1\right) \end{array} \right] \\ + \dfrac{c(\rho_f + \phi)s(\alpha_A + \beta - \rho_f - \psi_f)c(\alpha_A - \rho_f - \psi_f)e^{-b\psi_f}}{c(\alpha_A + \beta - \phi - \rho_f - \psi_f)} \end{array} \right\} \quad (10)$$

Similarly optimisation is carried out on variables ρ and ψ until the minimum $\mathbf{K_A}$ is found.

Active friction force, $\mathbf{F_A}$, is computed as $F_A = \frac{1}{2}\gamma H^2 K_A$

The failure force **F** from the CLUB model is obtained by substituting the equations (9) and (10) into equation (3).

2 Methodology

Soil models, (including those not discussed above) have the following common parameters:

- α: Tool angle measured relative horizontal,
- β: Soil surface angle measured relative to horizontal,
- **H**: Vertical insertion depth of the tool,
- ϕ: Internal friction angle of soil against soil,
- δ: Interface friction angle between soil and the tool,
- γ: Soil density,

α, β and **H** can be controlled while ϕ, δ and γ are inherent parameters of the soil. Soil properties and forces acting on the tool influence interaction between tool and terrain. Soil properties can therefore be estimated using measured forces acting on the tool. From equation (3) soil failure force **F** is computed as,

$$F = F_P - F_A = \frac{1}{2}\gamma H^2 \left(K_P(\alpha,\beta,\phi,\delta) - K_A(\alpha,\beta,\phi,\delta)\right)$$

To enable observation, acquisition and analysis of force data, micro-robotic soil-tool interaction experiments on three cohesion less-soils were formulated and carried out. The approach taken was to design and construct a **test rig**, incorporate into it a **Force-Torque sensing system** for measuring forces on the blade, set up a **data acquisition scheme** to record data from the sensor, select soil samples, set up and carry out robotic excavation experiments, compute the acquired Force-Torque data into **Soil Failure Force** data for different excavation blade settings and different sample soils and finally use the computed Soil Failure Forces with a **Soil parameter estimation technique** to **estimate properties** of the soil samples.

The next sections describe steps taken and equipment designed or selected that to achieve the set out project objectives.

2.1 Test rig design and construction

The test rig was designed to investigate the dynamical behaviour of the soil as it interacted with an excavation blade moving through it. Its specific function was to execute controlled robotic excavation, measure soil tool interaction forces and log data to a worksheet file for further analysis. It consisted of a soil bed to model the ground to be worked, a robotic manipulator to model motions of an excavator, a flat blade to model an excavation blade, a force-torque sensor to measure forces imparted to the blade, a data acquisition system to acquire data from the sensor and log it to file, as well as a computer system to control the robot and process the data. The designed and/or selected sets of equipment are further below described in more detail.

2.1.1 Robotics manipulator

Being readily available a Mitsubishi Movemaster EX RV-M1 manipulator system was selected to carry out the required robotic excavation. It is a vertically articulated 5 axis micro robot driven by DC servomotors through a toothed-belt transmission system. It has a lifting capacity 1.2 kg (11.8 N).

2.1.1.1 Communication and Control

The Movemaster RV-M1can be controlled by a hand-held teach pendant which monitors, programs and alters the robot's positions. It can also be programmed and controlled using a standard personal computer equipped with a serial and/or parallel interface. All five axes can be moved simultaneously. To control it with a PC, the PC was connected to the drive unit with either an RS-232C cable (although a Centronics cable can also be connected to the PC's parallel port). Commands, parameters and absolute position values are transferred from the computer to the drive unit's RAM via the interface. Normally current positions of each axis are registered individually by encoders and signaled to the drive unit. Limit switches determine the home position, used to synchronize the mechanical and electronic systems. The system has ten programmable speed levels.

2.1.1.2 Drive Unit

Included with the system, as standard equipment is the drive unit. It is a compact, modular power supply control unit, designed for easy servicing and transportation. It contains the CPU and power electronics required to control the robot. The drive unit communicates with the Movemaster RV-M1 via two 5 m cables. All interface ports and connections for peripheral equipment and process data as well as I/O are located on the rear panel. The unit is fitted with two standard interfaces (RS-232C and Centronics) for connection to personal computers

2.1.1.3 Hand gripper

The micro-robot was fitted with a motor operated hand that has standard force programmable hand gripping and opening features.

See appendix 8.1 for manufacturer's specifications of the RV-M1 Robot arm.

2.1.1.4 Outstanding Features

The Movemaster's outstanding features are; 5 degrees of freedom, not including the hand; DC servo motor drive; end position detection and overload monitoring; program development with personal computers connected via Centronics parallel or RS-232C serial port and power supply of 120 V AC, single phase, 50/60 Hz, 500 VA. See Appendix 8.1 for further specifications.

2.1.1.5 Robot programming

Programming and controlling the robot using a PC through a serial interface was more flexible and provided means to calculate tool positions beforehand. This approach was therefore preferred to the teach pendant. MATLAB MEX functions enabled the Movemaster commands to be embedded into the MATLAB environment making interfacing as well as programming of the robot flexible. Movemaster commands, classified according to their functions, were explored leading to selection of position and motion control commands because of their simplicity. Trials with this category of position/motion control commands lead to selection of the MP (Move Position) command. It was appropriate in that it moves the end effecter to positions and orientations whose position and angle coordinates can be prescribed before hand. Orientations and positions near the robots singularity configurations could easily be avoided since the robot system would defect and issue warning a signal before a move was executed. Through trials the required settings of the blade in terms of operation speed and orientation were combined with an approximated tool path to define positions that had to be traversed to execute the excavation.

The approximated tool path was computed to move the tool from nest position to the beginning of the excavation cycle. Then, at the lowest speed to minimize disturbance of surrounding soil, to carefully insert blade into soil at a specified insertion angle and to a specified depth, at the highest speed to obtain effective reaction forces from soil to the blade, to move the blade through a horizontal distance enough to fail the soil and finally retract the blade and position it for the next cycle. To carry out soil-tool friction angle estimation the excavation blade was moved to the 90^0-orientation position (shown in section 4 of figure 3) so that a rigid flat plate whose surface was evenly glued with sand could be manually rubbed against it. The soil failure force was assumed to be the maximum force imparted to the blade during the horizontal stroke of the excavation cycle shown in section 3 of figure 3.~~section~~. Figure 3 shows positions through which the blade traverses during excavation and the position for estimation of the soil tool interface friction.

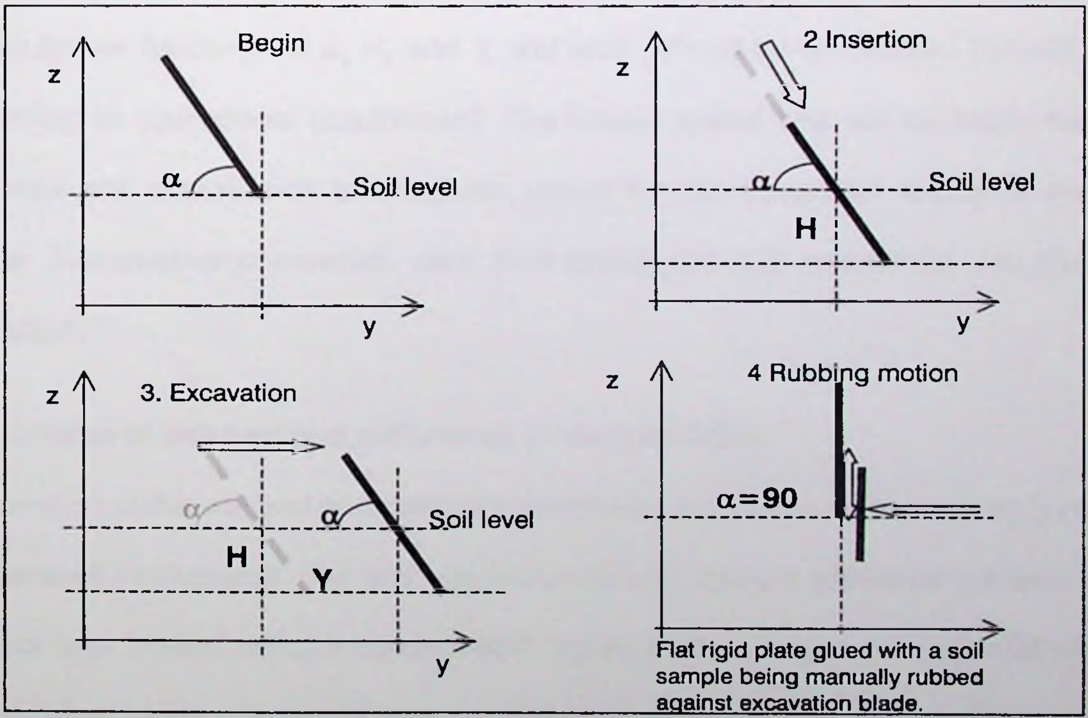

FIGURE 3. EXCAVATION CYCLE POSITIONS AND HAND RUBBING

Command format

The "Move position" command input format is **MP[<X-axis coordinate>], [<Y-axis coordinate>], [<Z-axis coordinate>], [<Pitch angle>], [<Roll angle>].** (Adapted from the RV-M1 Installation and operation manual)

A sample command is **MP 0, 400, 360, -45, -6**

Defining of positions;

Positions were defined according to the robot's world coordinate system. Blade insertion was along the robot's Z-axis, the horizontal stroke of excavation was set along the robots Y-axis and movement along the X-axis was fixed and set to the zero-X-axis coordinate. To ensure soil failure for the soils under investigation, the horizontal distance **(Y)** traversed by the inserted blade was determined to be approximately 100mm. Positions were then computed as functions of α, **H**, and **Y** and later refined by calibration. Speeds were set according to operational requirement. The lowest speed was set for blade insertion to minimize soil disturbance and highest speed for the horizontal stroke to ensure soil failure. Movemaster commands were then developed and embedded into MATLAB for execution.

Preparation of soil bed and calibration of tool positions

Preparation of the soil bed and calibration of blade positions was done using conventional off-the-shelf instruments. The soil was homogenized using a bricklayer's trowel while the surface was leveled using a conventional "spirit level". Using a conventional proctractor the required blade orientation was calibrated by adjusting the tool post-pitch angle and externally measuring the insertion angle (α). Using a conventional "T-square", the blade width perpendicularity to the Y-axis was set by incrementally adjusting the tool-post roll angle. The position from which blade insertion started (just above the leveled soil surface) was set using a steel rule as a spacer gauge, to leave approximately 1mm to 2 mm clearance between the soil and the blade. Calibration of all these positions and had to be carried out for each coded experiment.

Sample positions computed and calibrated for one of the experiments coded as 15010 are:.

(0, 400, 235, -45, -6);	Just above soil surface
(0, 408.4, 225, -45, -6);	Insertion Depth 10mm, ALPHA = 90-(-45 + 85)= 50
(0, 500, 225, -45, -6);	Horizontal stroke approximately 100mm angle zero
(0, 400, 360, -45, -6);	Blade extraction stroke

Delays:

The way the Movemaster processes data causes some signals sent from MATLAB to be delayed as they pass through. Thus, in order not to consequently miss out on some of the commands, delays in fractions of seconds were applied to synchronize signals within the transmission pipeline.

Figure 4 shows how the robot control program flows. See appendix 8.2 for samples of MATLAB code that was developed and named according to experiment nomenclature.

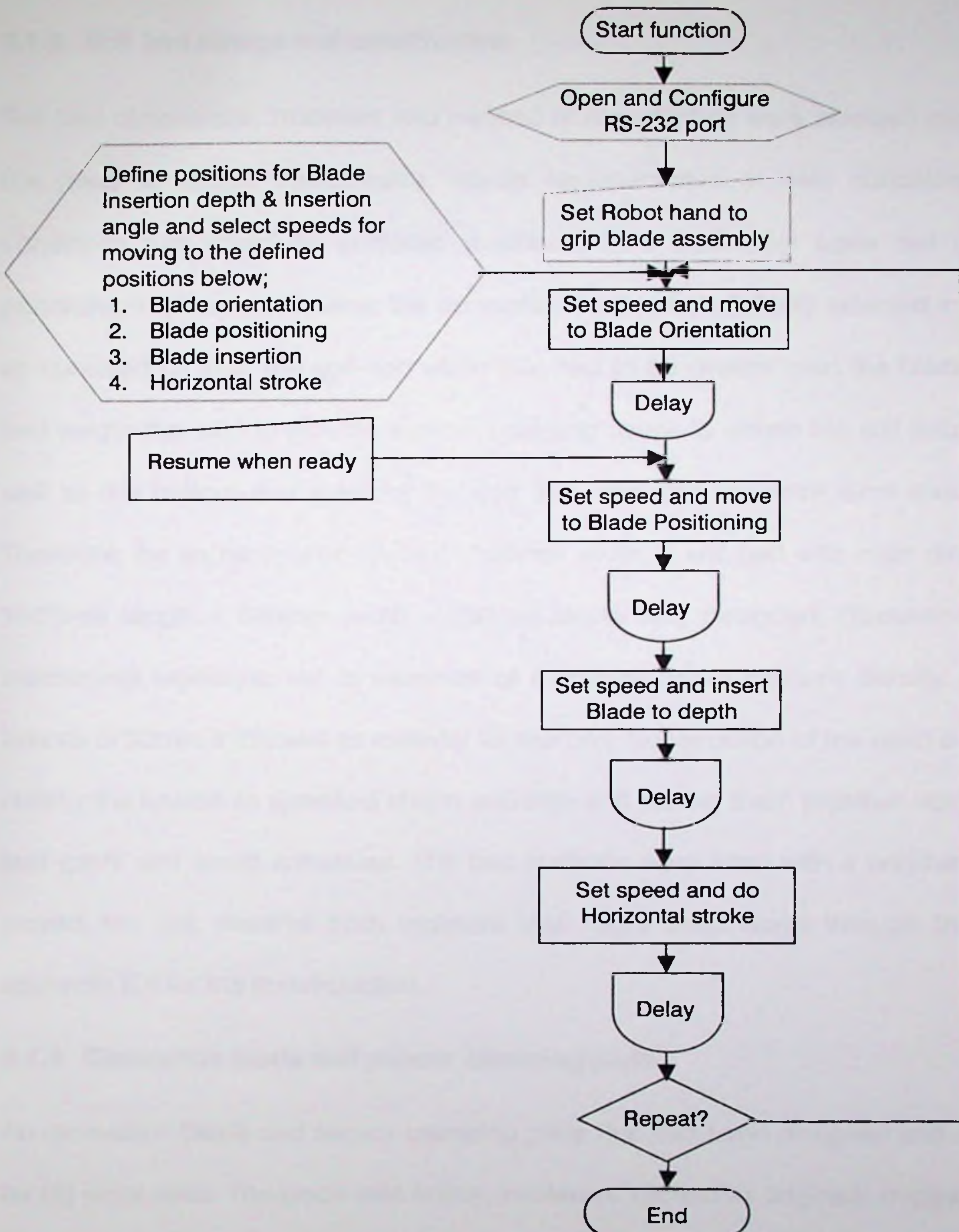

FIGURE 4. ROBOT CONTROL ALGORITHM

2.1.2 Soil bed design and construction

Soil bed dimensions, materials and method of manufacture were selected depending on the need to obtain interpretable results representative of field conditions and the conditions that could be achieved practically in a laboratory scale test rig. Factors pertaining to dimensions were; the excavation blade width (initially selected to be 150mm as specified by **[1]**), the soil bed width that had to be greater than the blade width, the bed length that had to provide sufficient digging space to obtain the soil failure force, as well as the bottom and sides of the bed that must not influence force measurements. Therefore, for an excavation blade of 150mm width, a soil bed with main dimensions of 1000mm length x 500mm width x 200mm depth was designed. Discussions with the mechanical workshop led to selection of melamine faced medium density fiber (MDF) boards of 20mm thickness as material for the box. Construction of the open box included cutting the boards to specified shape and size and joining them together using dowelled butt joints and wood adhesives. The box surfaces were lined with a polythene sheet to protect the box material from moisture that might seep down through the soil. See appendix 8.4 for the construcction.

2.1.3 Excavation blade and sensor clamping plate

An excavation blade and sensor clamping plate that had been designed and constructed by **[4]** were used. The blade was 50mm instead of 150mm as originally suggested by **[1]**. According to **[4]**, the blade/sensor assembly had been carefully designed and constructed to ensure that the sensor fitted on the blade and was able to register forces applied in desired directions. This was good since it was later discovered that the available soil samples would not fill up the designed box. Since the blade width had been reduced to 50mm, half the length of the box was more than sufficient to obtain the soil failure force. So the soil box was divided into two equal lengthwise partitions. As a result two soil samples could now be filled into the soil bed at a time.

2.1.4 Force Torque Sensor and DAQ

An SI-80-4, FT04671 DAQ/FT sensor system procured from ATI-Industrial Automation **[www.ati-ia.com]** was selected. It measures 6-axis forces and torques with maximum single axis loads $F_{xmax}=F_{ymax}=(+/-)$ 870N, $F_{zmax}=(+/-)$ 2700N, and $T_{xmax}=T_{ymax}=T_{zmax}=(+/-)$ 21Nm. It consists of a transducer, a shielded high-flex cable, and an intelligent ISA or stand-alone controller. The compact and rugged monolithic transducer uses silicon strain gauges to sense forces. The transducer's silicon strain gauges provide high noise immunity and allow high overload protection. The sensor produces an output that can be read by a data acquisition card that has six channels available. Thus it can be integrated with a PC to create a flexible system. See appendix 8.5 for manufacturer's description.

2.1.5 Data acquisition card

A National Instrument **[www.ni.com]** data acquisition card NI 6013 DAQ, being a multifunction I/O device for PCI Bus computers, was procured and installed into a Pentium III PC. It features 16 channels (8 of which are differential) of 16-bit analogue input, a 68-pin connector, and 8 lines of digital I/O. It uses the NI data acquisition system-timing controller (DAQ-STC) for time related functions. Lab VIEW 6i which is an application development environment (ADE) and NI-DAQ which is an extensive library of functions that can be called from any ADE allowed use of features of the NI 6013 DAQ. The NI-DAQ function library carried out many of the complex interactions, such as programming interrupts, between the computer and the DAQ hardware. Figure 5 shows the relationship among conventional programming environments, the functions library and the hardware.

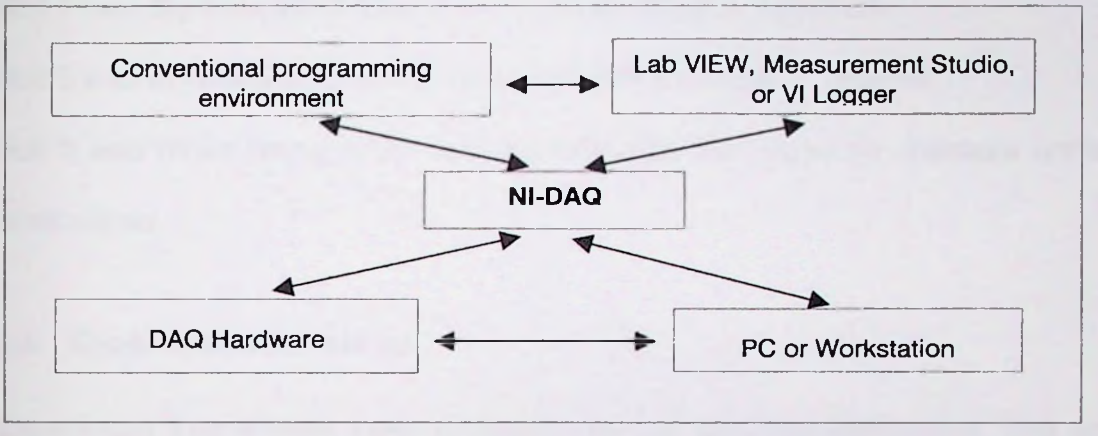

FIGURE 5. ADE, N-DAQ AND HARDWARE (ADAPTED FROM NI-DAQ INSTALLATION MANUAL) Shows the relationship among the Programming Environment, NI-DAQ and the Hardware

2.1.6 Manual Robot trolley and corresponding track,

A manual mobile trolley and corresponding tracks was partially designed with the intention to encode movement of the robot base thus simulating movement by track or wheels of an excavator machine in the field. Had it been completed it would also have made the test rig mobile. Due to lack of time the design and construction could not be completed. Instead the robot and the soil box were both set onto a robust workshop bench. Horizontal strokes of the excavation cycle were therefore accomplished by programming the robot to move between computed tool positions. See Appendix 8.3 for the intended trolley, tracks and sand box design and appendix 8.4 for photographs of the test rig that was actually used.

2.2 Soil samples

Three soil samples from Leighton Buzzard/Garside were procured and used in the excavation experiments. For identification they were named soil 1, soil 2 and soil 3. They were specified by the supplier's brochure as;

Soil.1 was dry fine-grained sand specified as NO 60 – 15/07/03.

Soil 2 was dry medium grained sand specified as 14/25 – 16/07/03

Soil 3 was moist fine-grained sand specified as Iron sand. Its moisture content was not determined.

2.3 Experimentation set up

Experiment instruments were arranged, set up and interconnected. The soil bed was placed onto a robust workshop bench and filled with soil samples. The RV-M1 robot was aligned and bolted down onto the bench. The excavation blade attached to the force-torque sensor was gripped by the robot's motor operated hand. An RS-232 serial port connection was established between the PC and the robot. Communication between the installed data acquisition card, the Force sensor and the PC was established. Figure 6 is a schematic drawing of the experiment instrumentation and connections.

2.4 Experiment Procedure

Experiments were carried out on the sample soils for different angles and depths of blade insertion and for soil tool interface friction. Codes developed to identify particular experiments denoted soil number, blade insertion depth, blade insertion angle and trial number. To validate the experiment and make initial soil sample conditions uniform two trials were carried out for each set. As an example code 150101 stands for soil 1, 50° blade insertion, 10mm blade insertion depth and trial 1

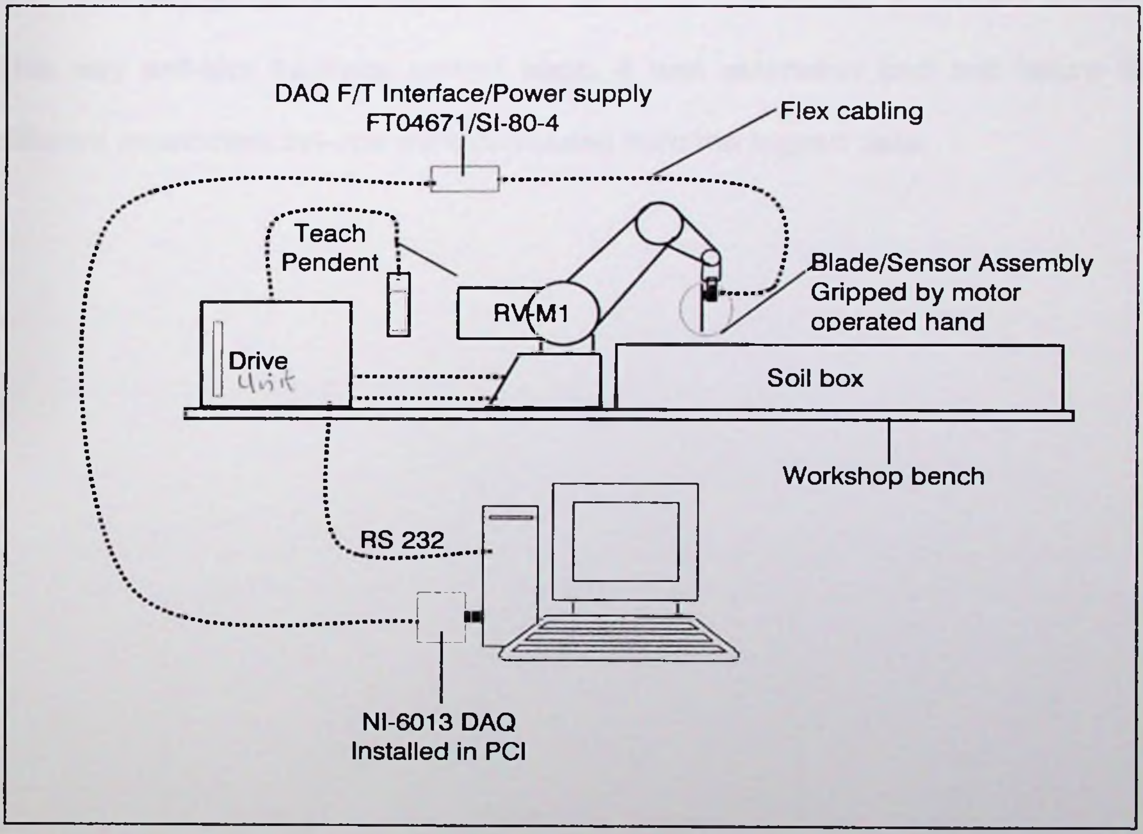

FIGURE 6. EXPERIMENT INSTRUMENTATION.

2.4.1 Steps followed in carrying out the experiments

I. Soil densities γ were estimated by weighing 500ml of soil samples

II. Two software packages, MATLAB and LabVIEW were run concurrently.

- Using MATLAB, appropriately defined functions (ALPHA<code >) were called to control the robot movements,
- Using LabVIEW and NI-6013 DAQ, data from the force sensor was collected (acquired) and subsequently logged onto appropriately named worksheet files, namely (ALPAHA<code*>.xls).

This way soil-tool interface friction angle δ was estimated and soil failure forces for different experiment set-ups were computed from the logged data.

3 Experiment results and discussions.

Raw data recorded from soil density estimation γ, soil-tool interface friction angle estimation δ and robotic excavation experiment settings, α and **H** was logged onto files that were named to designate the unique experiment set-ups. File names for experiment results of soil-tool interface friction angle estimation and for soil excavations data are respectively shown by the tables in figures 8 and 11.

3.1 Soil density estimation results.

Weighing 500ml of representative soil samples and computing the results into standard units accomplished soil density estimation. The supplier's density specifications are when the soils are in maximum compaction state as compared to the loose state when experiments for this project were being carried. Figure 7 shows soil density data for the project as compared to suppler specifications data.

Soil code	Soil Sample weight (kg)	Computed density (Mg/m^3)	Density specified by supplier (Mg/m^3)
1	0.8375	1.675	2.64
2	0.8035	1.607	2.64
3	0.7192	1.438	2.75

FIGURE 7. TABLE OF SOIL DENSITY DATA

3.2 Estimation of Soil Tool friction angle

Worksheet files named as below contained the data used to compute the soil-tool interface friction angle.

Soil code	Data sheet name (Last digit stands for 1st trial)	Data sheet name (Last digit stands for 2nd trial)	Data sheet name (Last digit stands for 3rd trial)
	DELTA11	DELTA12	DELTA13
	DELTA21	DELTA22	DELTA23
	DELTA31	DELTA32	DELTA33

FIGURE 8. WORKSHEET FILES FOR RESULTS OF SOIL-TOOL INTERFACE FRICTION ANGLE

Equation (2) was applied to estimate soil-tool friction angle δ. When a flat rigid plate glued with soil sample was manually rubbed against excavation blade (section 4 of figure 3). **S** is the resultant force on the blade in the robot's Z-axis direction and σ is the resultant force in the Y-axis direction. Replacing ϕ with δ and considering the blade and force sensor geometrical construction equation (11) was developed.

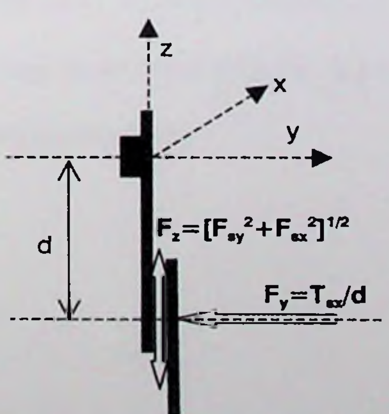

FIGURE 9. FORCE/TORQUE SENSOR & BLADE ASSEMBLY

Logic of the blade geometrical construction and the vertical up and down direction of the rubbing motion (figure 9) implies that out of the six components picked by the sensor only F_{sy}, F_{sx} and T_{sx} are relevant for δ estimation, giving,

$$\delta = \tan^{-1}\left[\frac{s}{\sigma}\right] = \tan^{-1}\left[\frac{F_z}{F_y}\right] = \tan^{-1}\left[\frac{(F_{sy}^2 + F_{sx}^2)^{\frac{1}{2}}}{(T_{sx}/d)}\right] \qquad (11)$$

Soil-tool friction angles for the three soils were estimated as the average of the peak points of graphs generated when equation (11) was applied to data logged into files named in figure 8. The estimated values are shown in figure 10.

Soil code	Trial1	Trial2	Trial3	Average
1	34	50	42	43
2	32	33	32	32
3	33	30	36	33

FIGURE 10. ESTIMATED SOIL-TOOL FRICTION ANGLE, δ.

The following three pages are the graphs used to estimate the soil-tool interface friction angle δ, for the three sample soils.

DELTA 11: Estimated delta for soil 1, trial 1 = 34

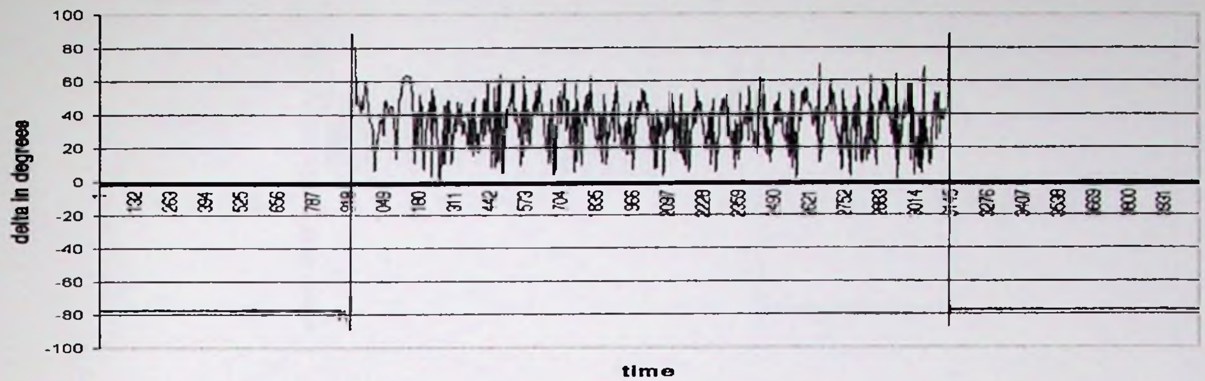

The average of the peak points between t=1200 to t=3000 gives a good estimate of δ

DELTA 12: Estimated delta for soil 1 trial 2 = 50

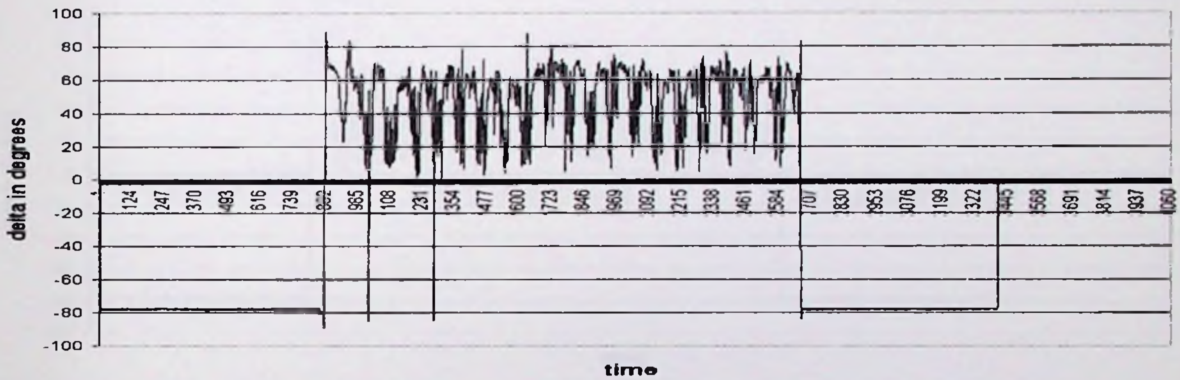

The average of the peak points between t=1300 to t=2500 gives a good estimate of δ.

DELTA 13: Estimated delta for soil 1 trial 3 = 42

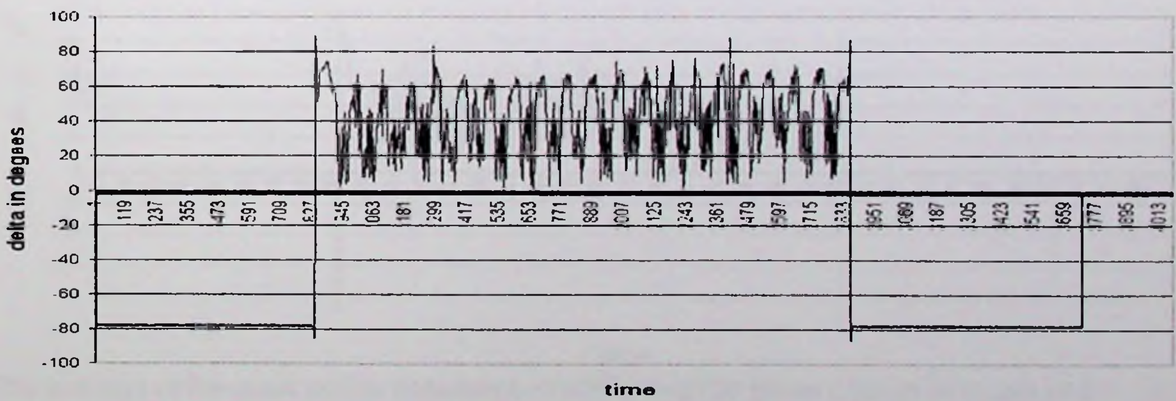

The average of the peak points between t=1000 to t=2700 gives a good estimate of δ.

DELTA 21 Estimated delta for soil 2 trial 1= 32

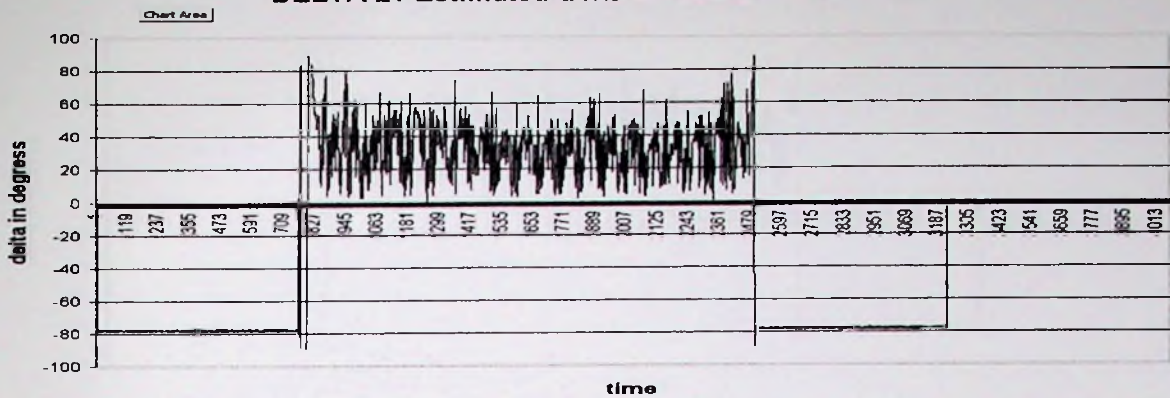

The average of the peak points between t=900 to t=2300 gives a good estimate of δ

DELTA 22 Estimated delta for soil 2 trial 2 = 33

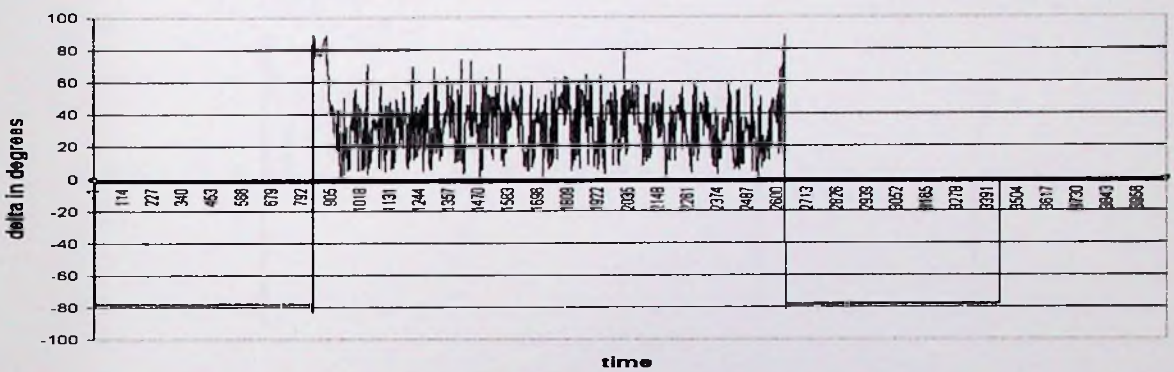

The average of the peak points between t=900 to t=2500 gives a good estimate of δ

DELTA 23: Estimated delta for soil 2 trial 3 = 32

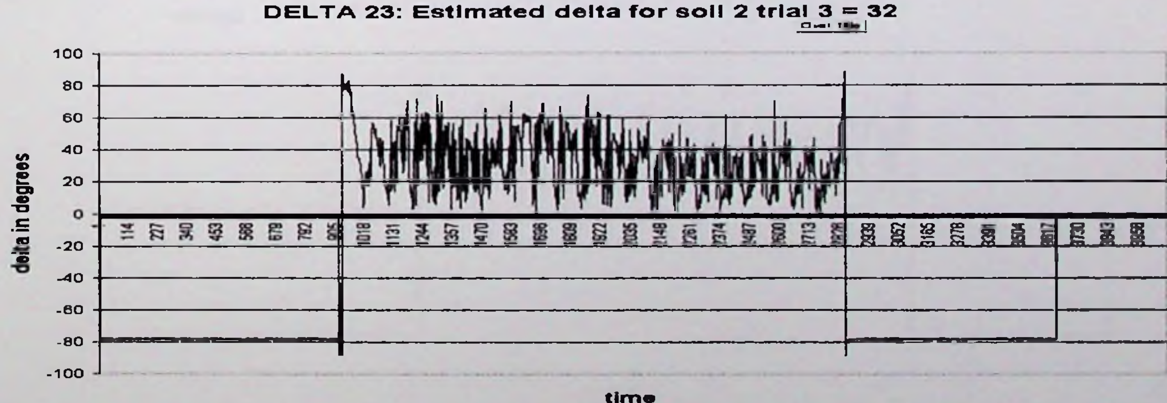

The average of the peak points between t=1100 to t=2700 gives a good estimate of δ

DELTA 31: Estimated delta for soil 3 trial 1 = 33

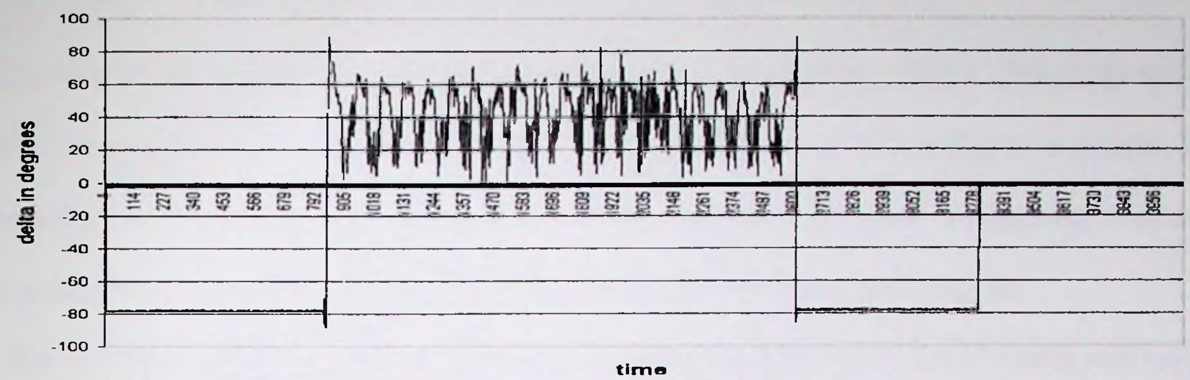

The average of the peak points between t=1100 to t=2700 gives a good estimate of δ

DELTA 32: Estimated delta for soil 3 trial 2 = 30

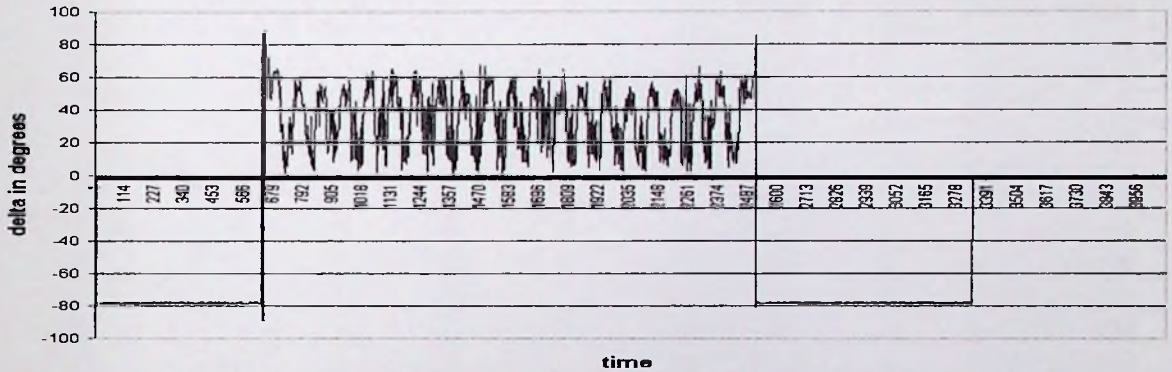

The average of the peak points between t=860 to t=2400 gives a good estimate of δ

DELTA 33: estimated delta for soil 3 trial 3 = 36

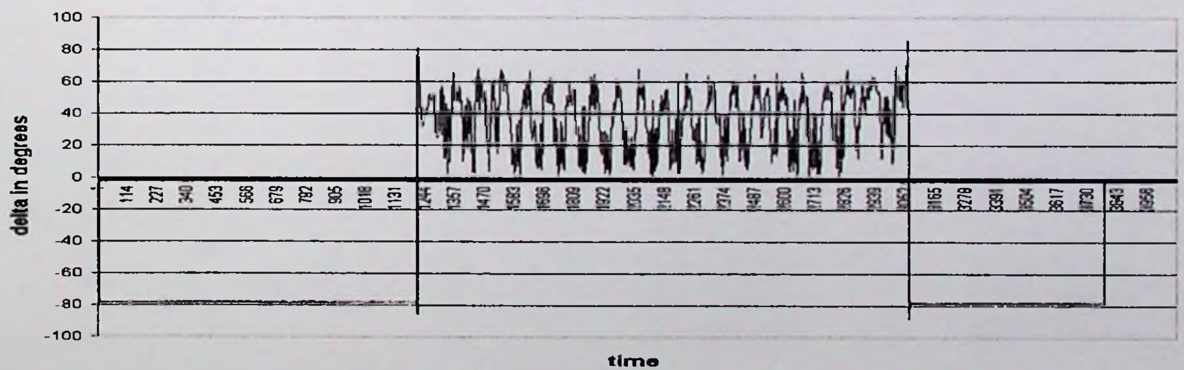

The average of the peak points between t=1300 to t=3000 gives a good estimate of δ

3.3 Soil Failure Force Results

Soil failure force was computed from excavation experiments results. The table in figure 11 shows unique codes given to each individual experiment according to soil type, blade insertion depth and angle. To validate the results two trials were conducted. The codes are also the file names of worksheet files into which raw data was logged.

Soil code	Blade insertion Angle (degrees)	Blade Insertion depth in mm	Results code with Last digit for 1st trial	Results code with Last digit for 2nd trial
1	50	10	ALPHA150101	ALPHA150102
		20	ALPHA150201	ALPHA150202
	60	10	ALPHA160101	ALPHA160102
		20	ALPHA160201	ALPHA160202
	70	10	ALPHA170101	ALPHA170102
		20	ALPHA170201	ALPHA170202
	80	10	ALPHA180101	ALPHA180102
		20	ALPHA180201	ALPHA180202
	90	10	ALPHA190101	ALPHA190102
		20	ALPHA190201	ALPHA190202
2	50	10	ALPHA250101	ALPHA250102
		20	ALPHA250201	ALPHA250202
	60	10	ALPHA260101	ALPHA260102
		20	ALPHA260201	ALPHA260202
	70	10	ALPHA270101	ALPHA270102
		20	ALPHA270201	ALPHA270202
	80	10	ALPHA280101	ALPHA280102
		20	ALPHA280201	ALPHA280202
	90	10	ALPHA290101	ALPHA290102
		20	ALPHA290201	ALPHA290202
3	50	10	ALPHA350101	ALPHA350102
		20	ALPHA350201	ALPHA350202
	60	10	ALPHA360101	ALPHA360102
		20	ALPHA360201	ALPHA360202
	70	10	ALPHA370101	ALPHA370102
		20	ALPHA370201	ALPHA370202
	80	10	ALPHA380101	ALPHA380102
		20	ALPHA380201	ALPHA380202
	90	10	ALPHA390101	ALPHA390102
		20	ALPHA390201	ALPHA390202

FIGURE 11. DATA LOG OF EXCAVATION EXPERIMENTS.

3.3.1 Static Equilibrium Analysis

Static equilibrium analysis of forces acting on the excavation blade as it executes the horizontal stroke of excavation (figure 3 position 3) is used to compute the soil failure force. Since Forces in the XZ plane are negligible only forces in the YZ plane were considered. Thus out of the six components picked by the sensor only F_z, and T_x are relevant for soil failure force computation. Resultant forces at discrete points in time were plotted on graphs. Soil failure force is the maximum picked from the graphs.

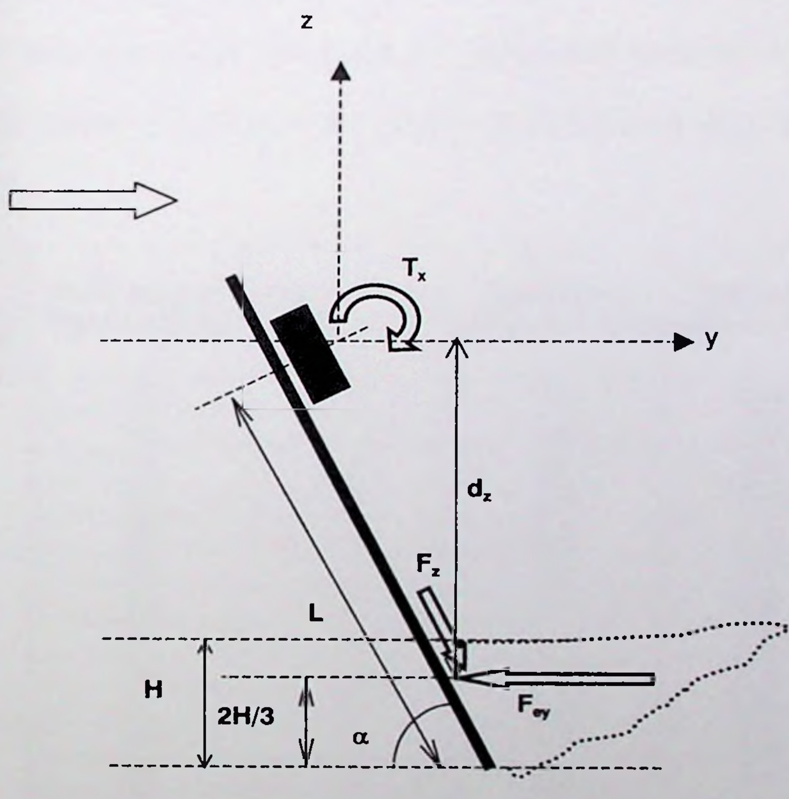

FIGURE 12. STATIC EQUILIBRIUM ANALYSIS OF EXPERIMENTAL SOIL-TOOL INTERACTION FORCES

Consideration of the blade and force/torque sensor geometrical construction in figure 12 computes resultant force, **F** as;

$$F=\left[F_{ey}^{2}+F_{z}^{2}\right]^{\frac{1}{2}},\qquad F_{ey}=\frac{T_x}{d_z},\qquad d_z=L\sin\alpha-\frac{2}{3}H$$

$$\Rightarrow F=\sqrt{\left(\frac{T_x}{\left(L\sin\alpha-\frac{2}{3}H\right)}\right)^{2}+F_z^{2}} \qquad (12)$$

Where F_z and T_x are the relevant sensor data from the logged data files and d_z is a geometrical dimension of the flat blade. Applying equation (12) to the data files in table of figure 11 and picking off the maximum computed force as the Soil failure force gives results as shown in figures 13 for 10 mm blade insertion and figure 14 for 20 mm blade insertion.

Soil code	Blade insertion Angle (degrees)	Blade Insertion depth in mm	Soil Failure force, N, Trial 1	Soil Failure force, N, Trial 2	Average Soil Failure Force, N
1	50	10	3.80	3.50	3.65
	60	10	3.55	3.56	3.56
	70	10	5.64	5.76	5.70
	80	10	5.98	5.16	5.57
	90	10	5.98	5.63	5.81
2	50	10	4.68	4.27	4.48
	60	10	6.96	3.98	5.47
	70	10	5.50	4.50	5.00
	80	10	5.55	5.34	5.45
	90	10	6.16	6.52	6.34
3	50	10	4.54	5.20	4.87
	60	10	6.47	4.61	5.54
	70	10	8.26	5.27	6.77
	80	10	7.90	8.10	8.00
	90	10	13.32	12.20	12.76

FIGURE 13. SOIL FAILURE FORCES FOR 10 MM BLADE INSERTION DEPTH

Soil code	Blade insertion Angle (degrees)	Blade Insertion depth in mm	Soil Failure force, N, Trial 1	Soil Failure force, N, Trial 2	Average Soil Failure Force, N
1	50	20	7.63	7.10	7.37
	60	20	8.00	7.40	7.70
	70	20	10.90	10.90	10.90
	80	20	10.24	10.57	10.41
	90	20	11.70	10.86	11.28
2	50	20	9.33	7.80	8.57
	60	20	10.01	9.40	9.71
	70	20	10.93	8.90	9.92
	80	20	11.64	11.80	11.72
	90	20	16.32	16.20	16.26
3	50	20	10.46	10.63	10.55
	60	20	10.15	9.00	9.58
	70	20	13.96	13.25	13.61
	80	20	15.46	17.33	16.40
	90	20	26.84	23.88	25.36

FIGURE 14 SOIL FAILURE FORCES FOR 20 MM BLADE INSERTION DEPTH

The following 15 pages show graphs from which soil failure forces were picked. They are plots of the result from application of equation (12) to data files in figure 11.

Graphical results of Soil failure forces

Soil 1 Alpha 50

Effective Soil Failure Force F = 3.8 N
Data code 150101: Soil 1, alpha =50 degrees, H = 10mm, L = 100mm, sample 1

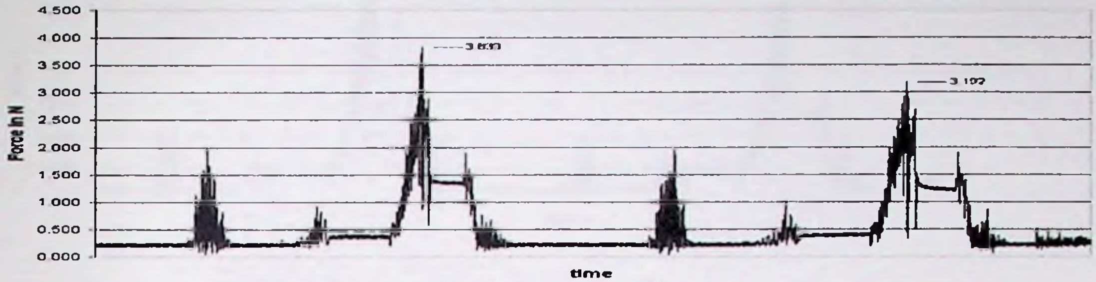

Effective Force on blade F = 3.5 N
Data code 150102: Soil 1, alpha =50 degrees, H = 10mm, L = 100mm, trial 2

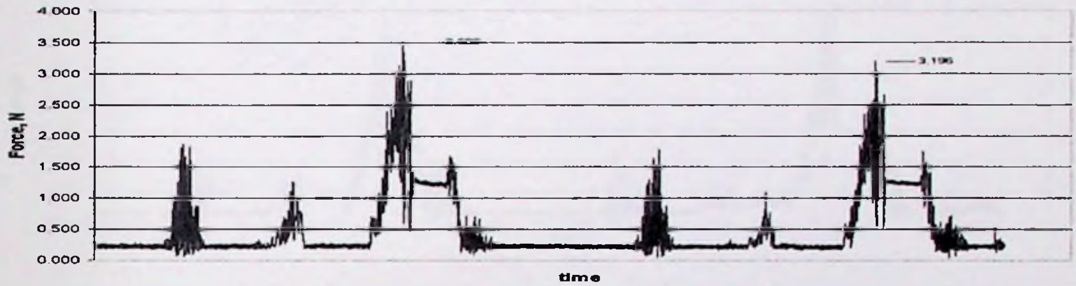

Effective Force on blade F = 7.63 N
Data code 150201: Soil type 1, alpha = 50 deg, H = 20mm, L = 100mm, Trial 1

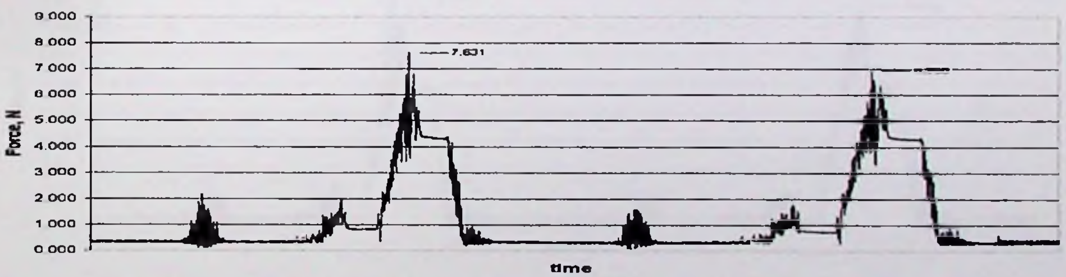

Soil Failure Force on blade F = 7.1 N
Data code 150202: Soil type 1, alpha = 50 deg, H = 20mm, L = 100mm, Trial 2

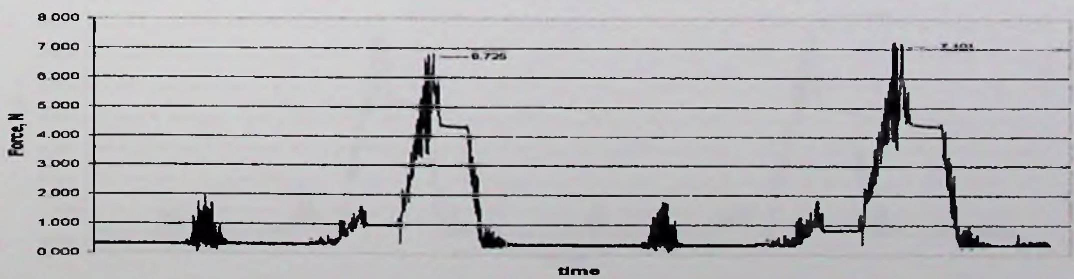

Soil 1 Alpha 60

Soil Failure Force, F = 3.55 N
Data code 160101: Soil type 1, alpha =60 deg, H = 10mm, L = 100mm, Trial 1

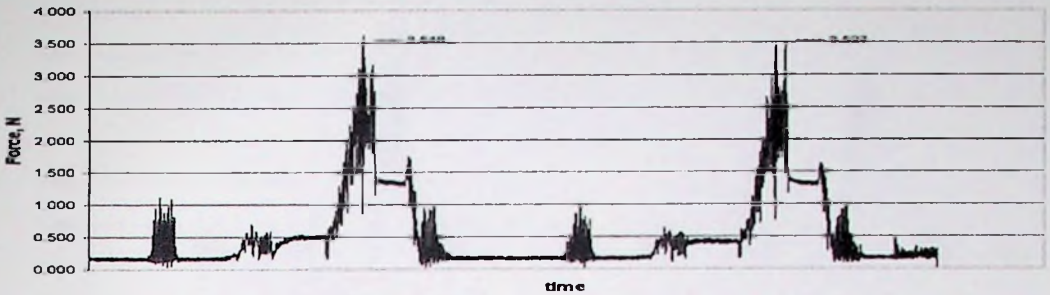

Soil Failure Force F = 3.56
Data code 160102: Soil type 1, alpha =60 deg, H = 10mm, L = 100mm, Trial 2

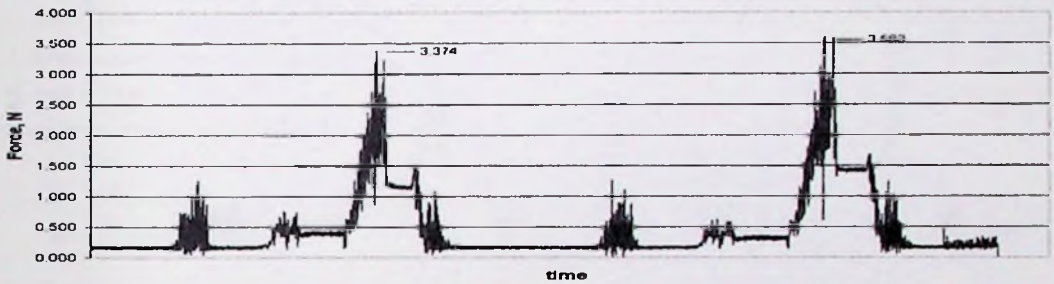

Soil Failure Force, F = 8 N
Data code 160201: Soil type 1, alpha =60 deg, H = 20mm, L = 100mm, Trial 1

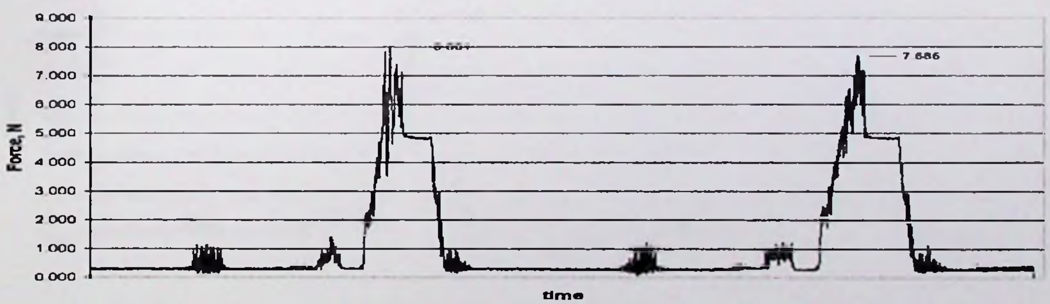

Soil Failure Force, F = 7.4
Data code 160202: Soil type 1, alpha =60 deg, H = 20mm, L = 100mm, Trial 2

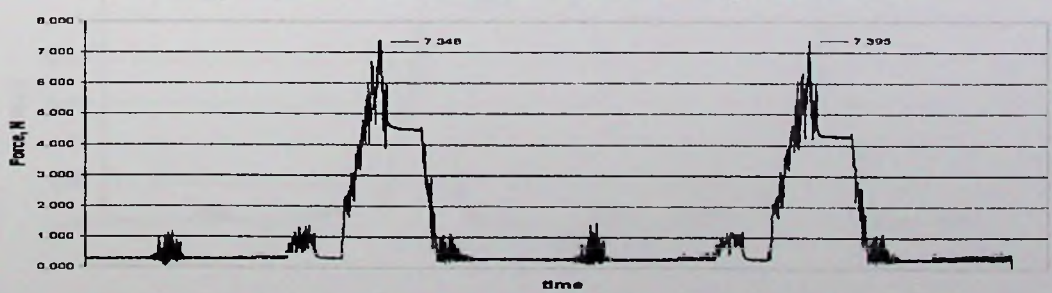

Soil 1 Alpha 70

Soil Failure Force, F = 5.64
Data code 170101: Soil type 1, alpha =70 deg, H = 10mm, L = 100mm, Trial 1

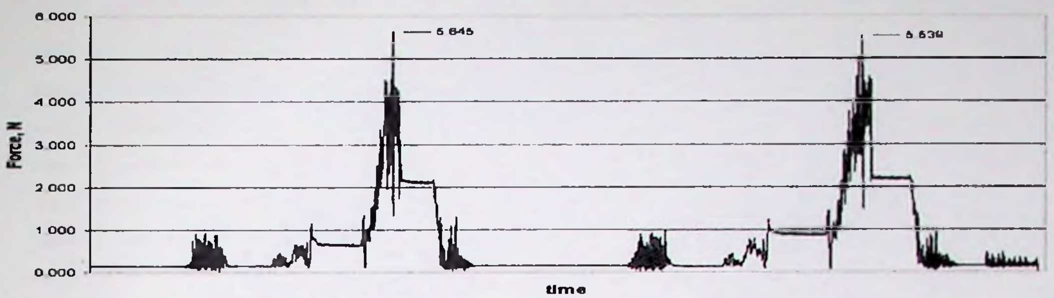

Soil failure Force F = 5.76 N
Data code 170102: Soil type 1, alpha =70 deg, H = 10mm, L = 100mm, Trial 2

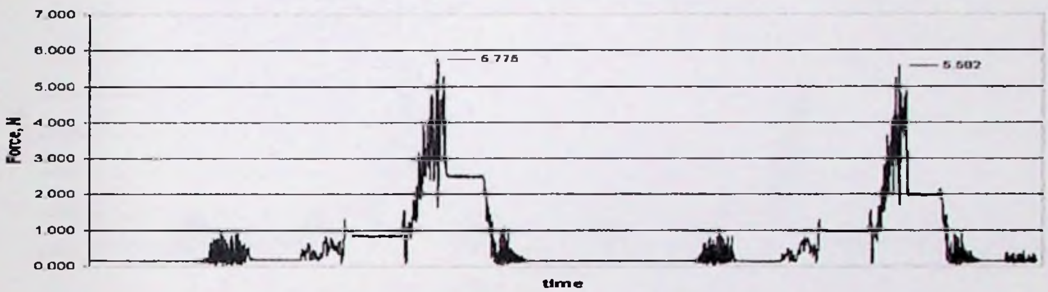

Soil Failure Force, F = 10.9 N
Data code 170201: Soil type 1, alpha =70 deg, H = 20mm, L = 100mm, Trial 1

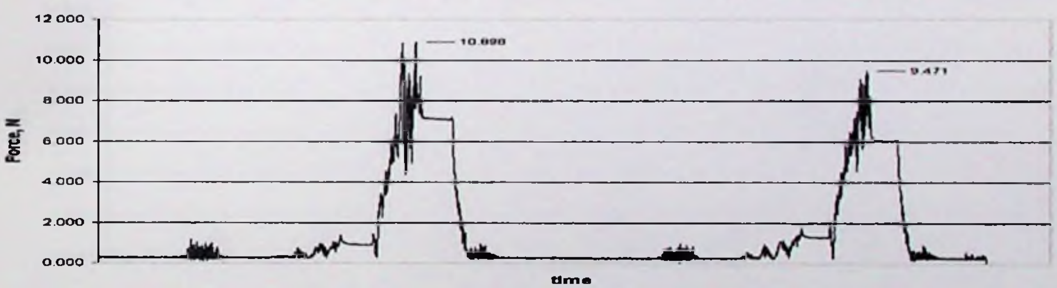

Soil Failure Force, F = 10.9 N
Data code 170202: Soil type 1, alpha =70 deg, H = 20mm, L = 100mm, Trial 2

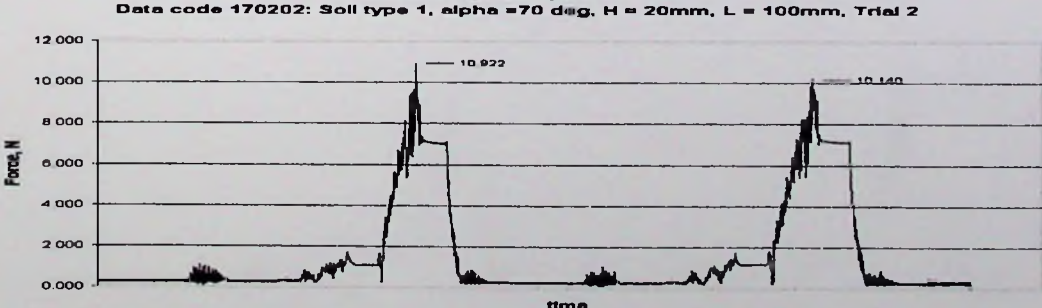

Soil 1 Alpha 80

Soil Failure Force, F = 5.98 N
Data code 180101: Soil type 1, alpha =80 deg, H = 10mm, L = 100mm, Trial 1

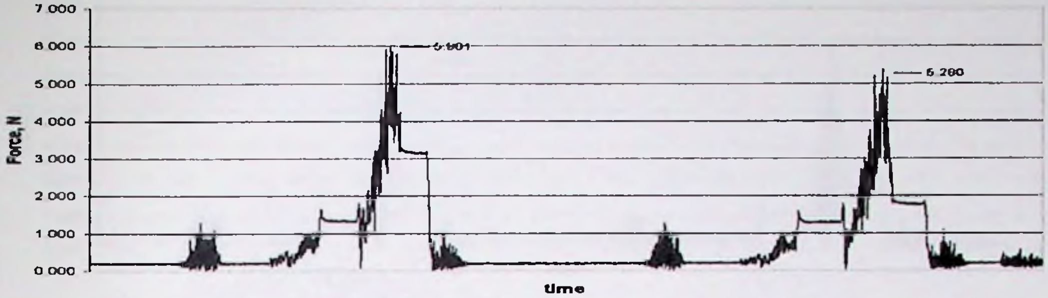

Soil Failure Force, F = 5.16 N
Data code 180102: Soil type 1, alpha =80 deg, H = 10mm, L = 100mm, Trial 2

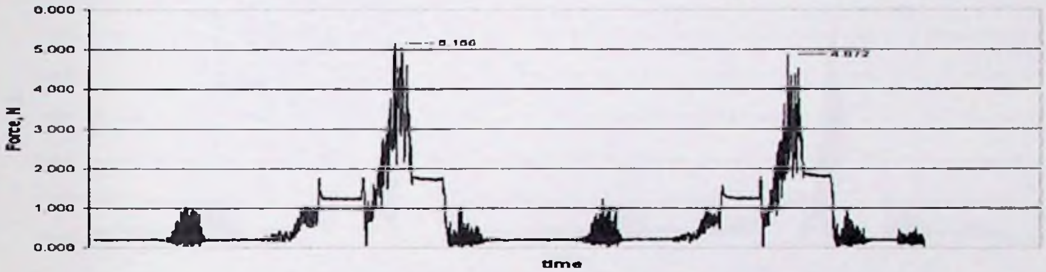

Soil Failure Force, F = 10.24 N
Data code 180201: Soil type 1, alpha =80 deg, H = 20mm, L = 100mm, Trial 1

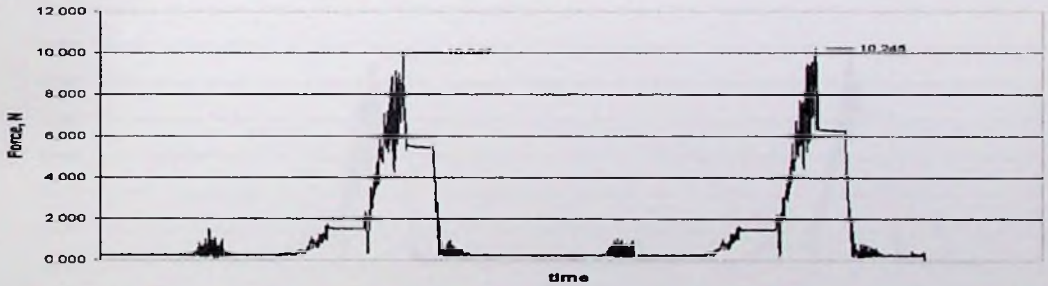

Soil Failure Force, F = 10.57 N
Data code 180202: Soil type 1, alpha =80 deg, H = 20mm, L = 100mm, Trial 2

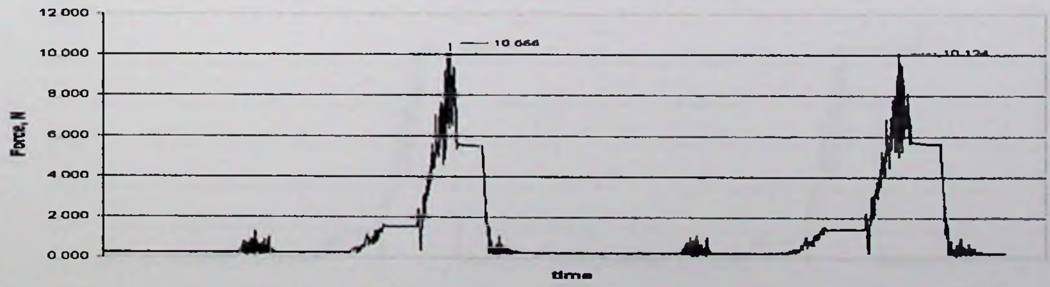

Soil 1 Alpha 90

Effective Soil failure Forc,e F = 5.98 N
Data code 190101: Soil type 1, alpha =90 deg, H = 10mm, L = 100mm, Trial 1

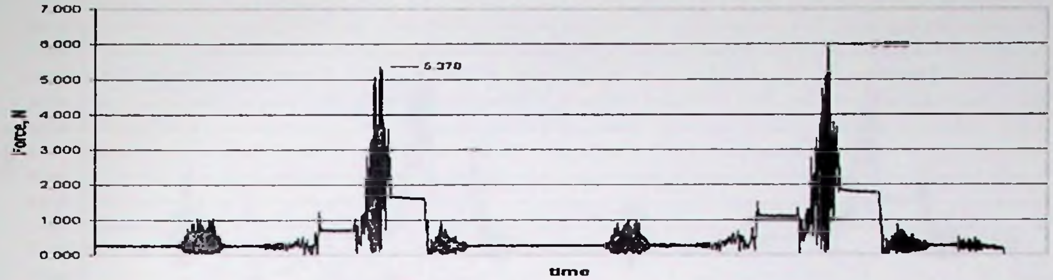

Soil failure Force, F = 5.63 N
Data code 190102: Soil type 1, alpha =90 deg, H = 10mm, L = 100mm, Trial 2

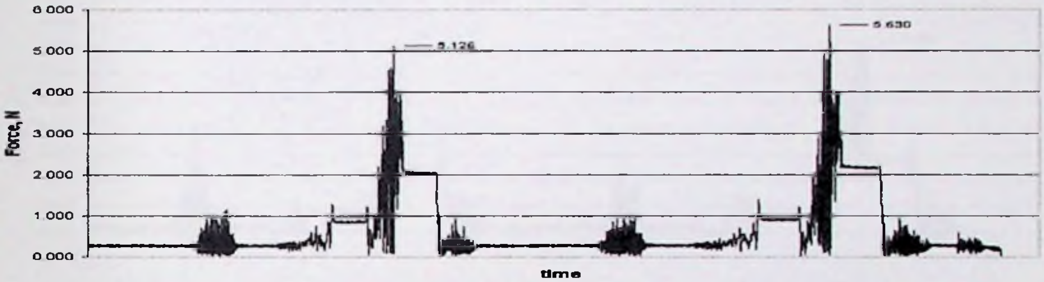

Effective Soil failure Force, F =11.7 N
Data code 190201: Soil type 1, alpha =90 deg, H = 20mm, L = 100mm, Trial1

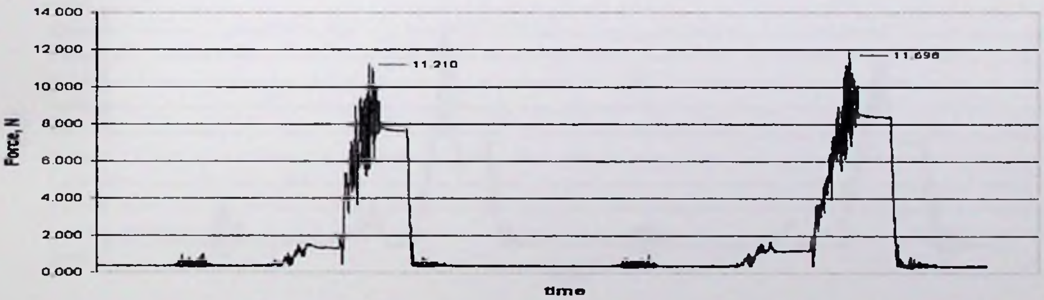

Soil Failure Force, F = 10.86 N
Data code 190202: Soil type 1, alpha =90 deg, H = 20mm, L = 100mm, Trial 2

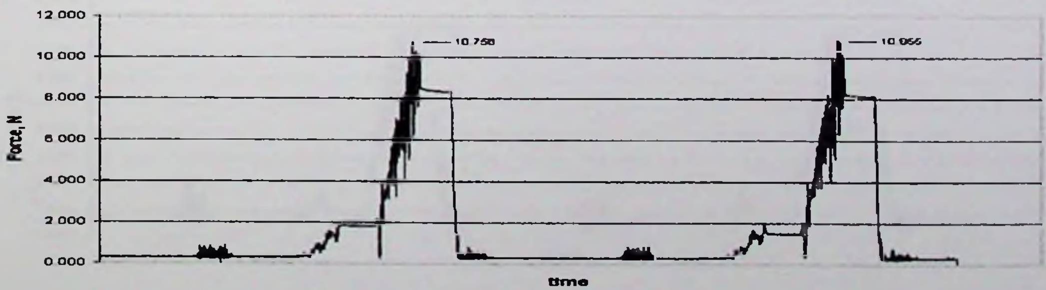

Soil 2 Alpha 50

Soil Failure Force, F = 4.68 N
Data code 250101: Soil type 2, alpha =50 deg, H = 10mm, L = 100mm, Trial 1

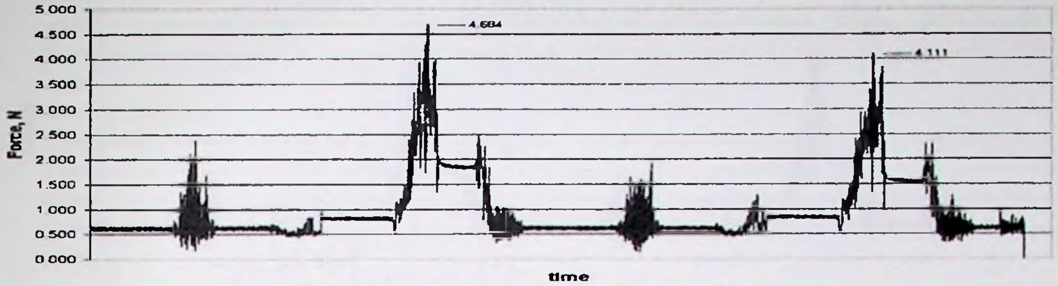

Soil Failure Force, F = 4.27 N
Data code 250102: Soil type 2, alpha =50 deg, H = 10mm, L = 100mm, Trial 2

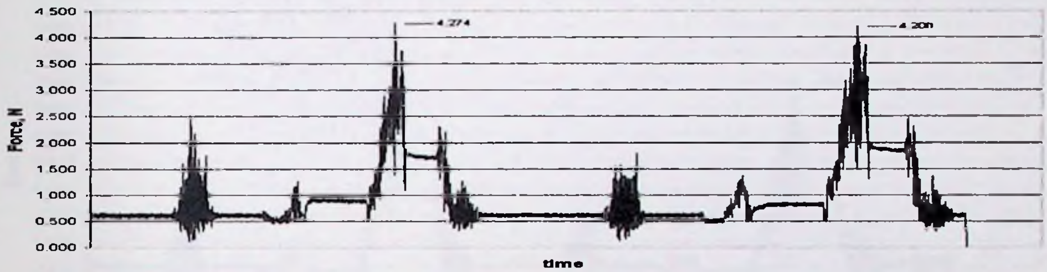

Soil Failure Force, F = 9.33 N
Data code 250201: Soil type 2, alpha =50 deg, H = 20mm, L = 100mm, Trial 1

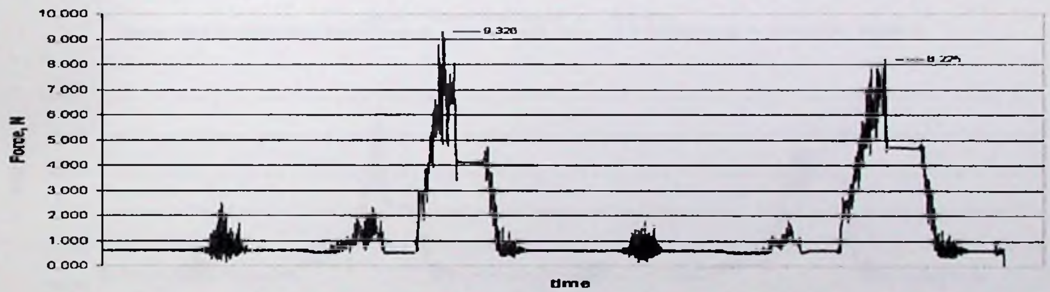

Soil Failure Force, F = 7.8 N
Data code 250202: Soil type 2, alpha =50 deg, H = 20mm, L = 100mm, Trial2

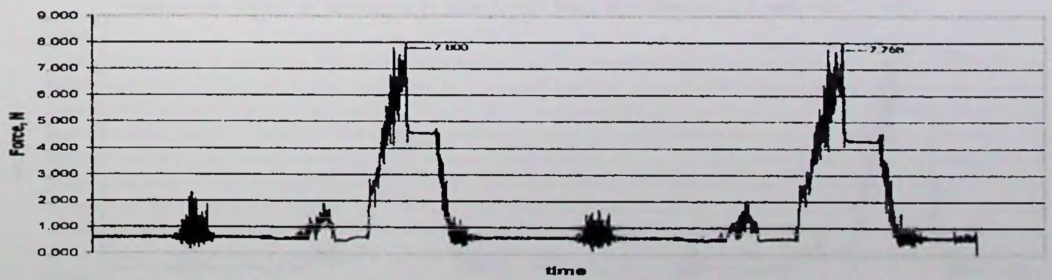

Soil 2 Alpha 60

Soil Failure Force, F = 3.96
Data code 260101: Soil type 2, alpha =60 deg, H = 10mm, L = 100mm, Trial 1

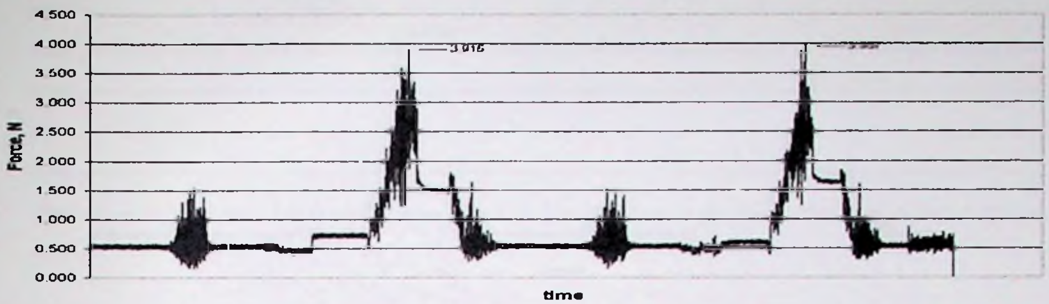

Soil Failure Force, F = 3.98 N
Data code 260102: Soil type 2, alpha =60 deg, H = 10mm, L = 100mm, Trial 2

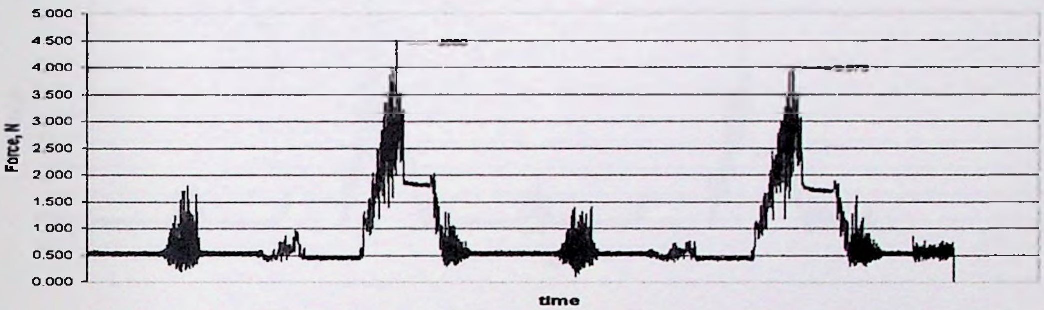

Soil Failure Force, F = 10.01 N
Data code 260201: Soil type 2, alpha =60 deg, H = 20mm, L = 100mm, Trial 1

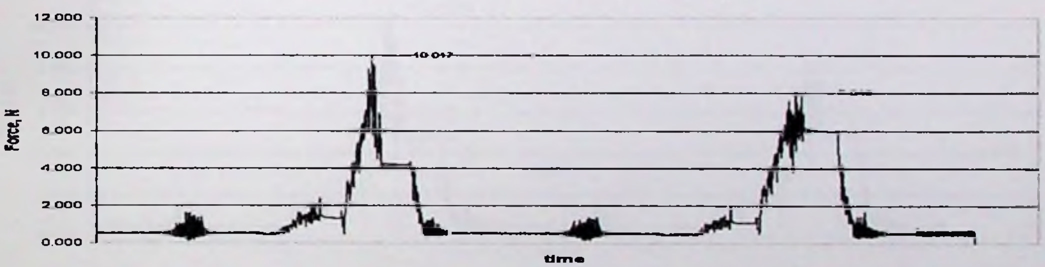

Soil Failure Force, F = 9.4 N
Data code 260202: Soil type 2, alpha =60 deg, H = 20mm, L = 100mm, Trial 2

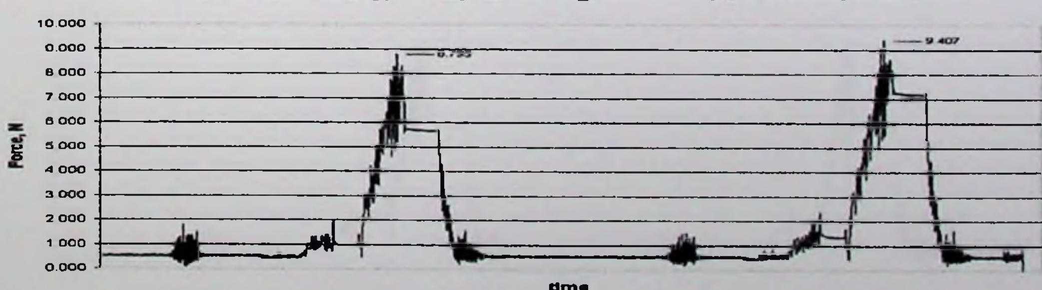

Soil 2 Alpha 70

Soil Failure Force on blade F = 5.5 N
Data code 270101: Soil type 2, alpha =70 deg, H = 10mm, L = 100mm, Trial 1

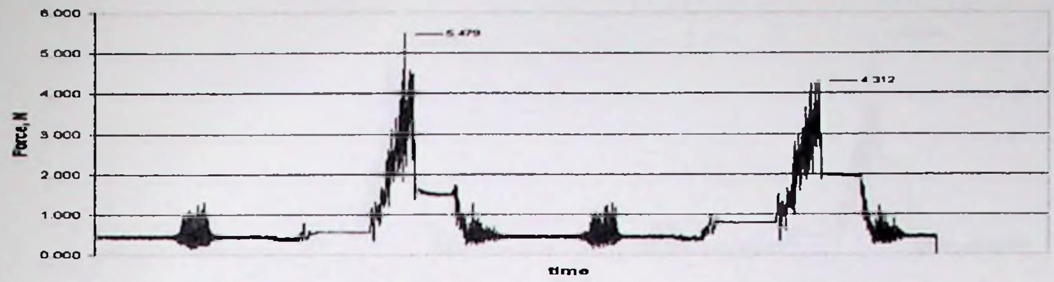

Soil Failure Force, F = 4.5 N
Data code 270202: Soil type 2, alpha =70 deg, H = 10mm, L = 100mm, Trial 2

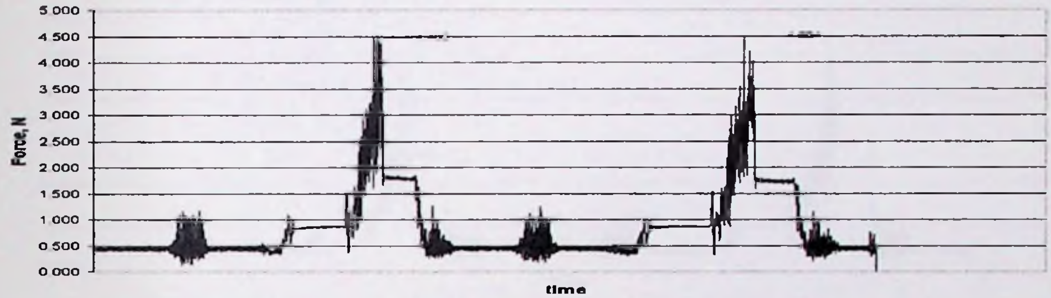

Soil Failure Force, F = 10.93 N
Data code 270201: Soil type 2, alpha =70 deg, H = 20mm, L = 100mm, Trial 1

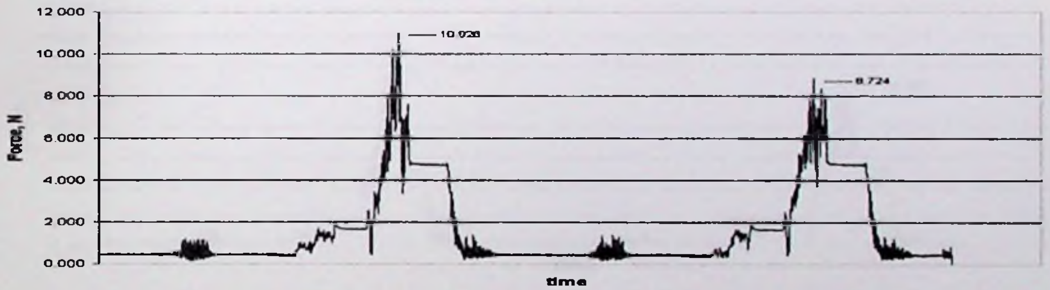

Soil failure Force F = 8.9 N
Date code 270202: Soil type 2, alpha =70 deg, H = 20mm, L = 100mm, Trial 2

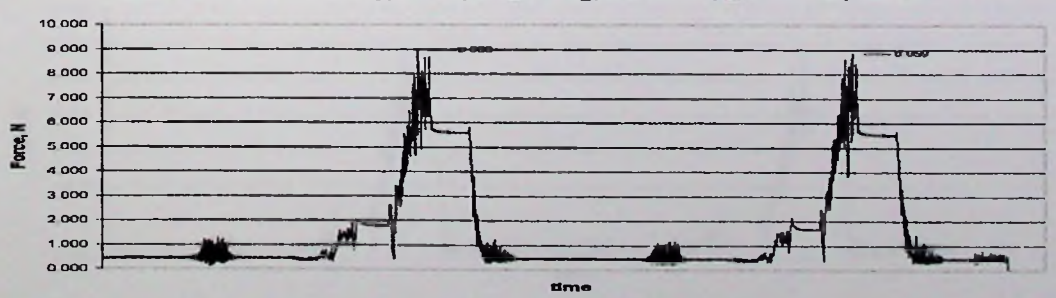

Soil 2 Alpha 80

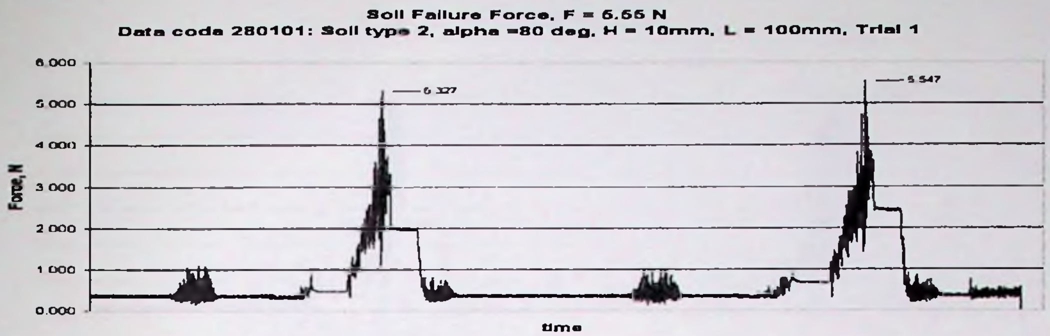

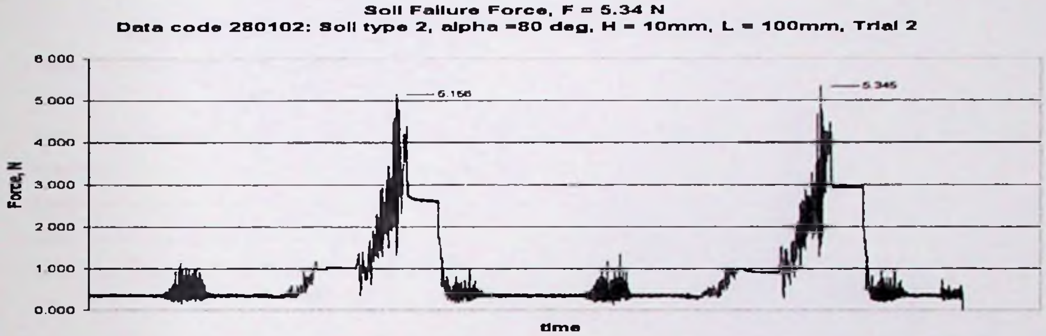

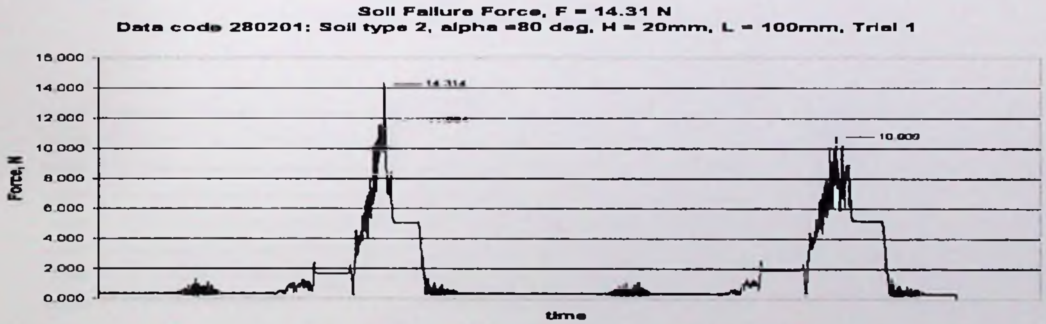

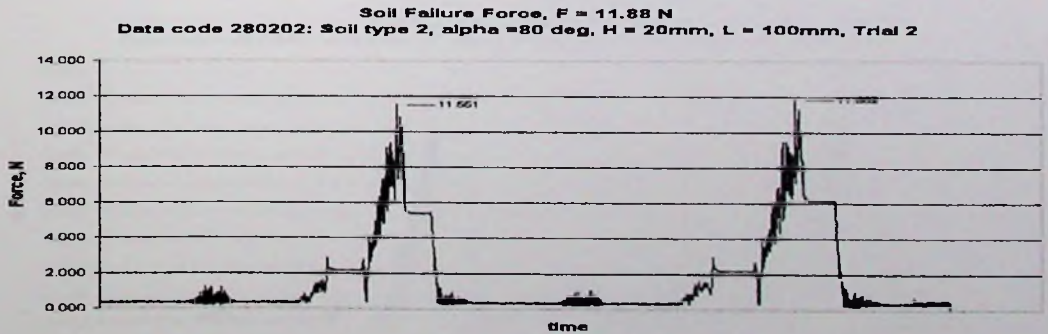

Soil 2 Alpha 90

Soil Failure Force, F = 6.16 N
Data code 290101: Soil type 2, alpha =90 deg, H = 10mm, L = 100mm, Trial 1

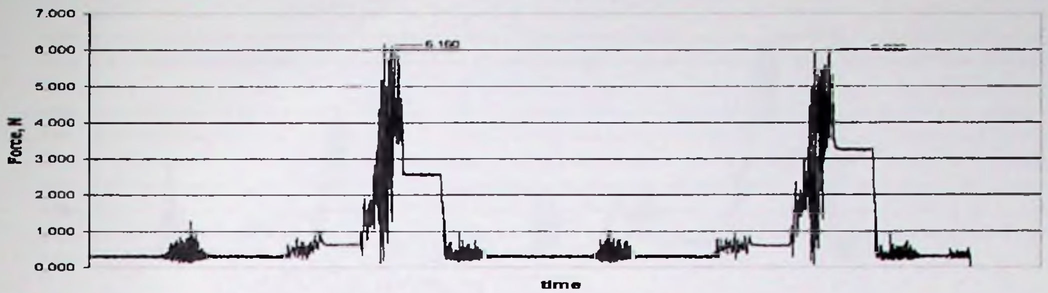

Soil Failure Force, F = 6.52N
Data code 290102: Soil type 2, alpha =90 deg, H = 10mm, L = 100mm, Trial 2

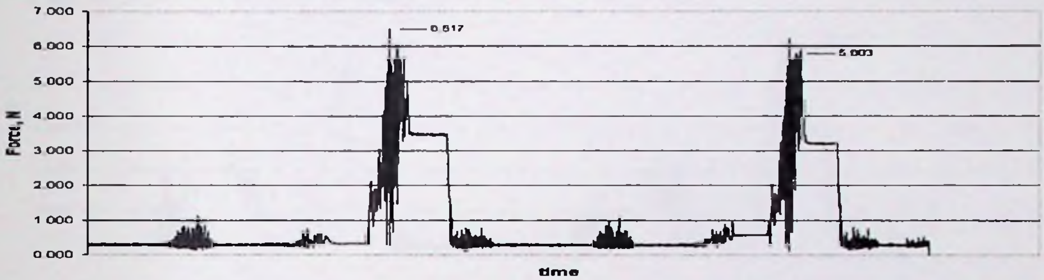

Soil Failure Force, F = 16.32 N
Data code 290201: Soil type 2, alpha =90 deg, H = 20mm, L = 100mm, Trial 1

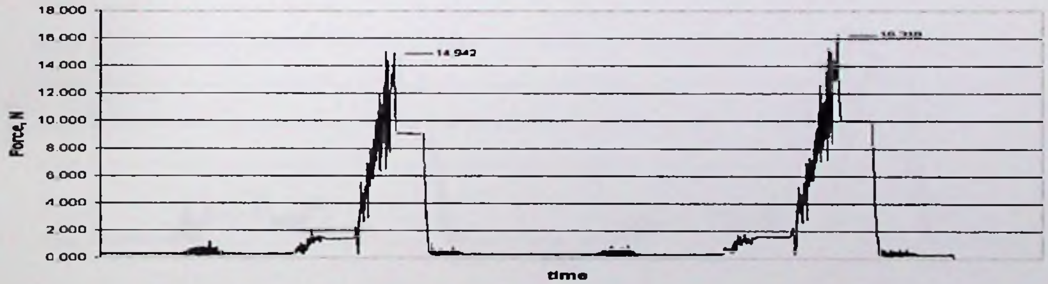

Soil Failure Force, F = 16.2 N
Data code 290202: Soil type 2, alpha =90 deg, H = 20mm, L = 100mm, Trial 2

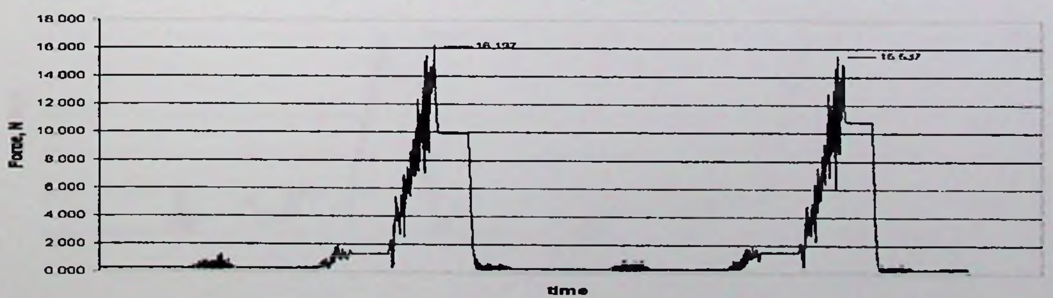

Soil 3 Alpha 50

Soil Failure Force, F = 4.54 N
Data code 350101: Soil type 3, alpha =50 deg, H = 10mm, L = 100mm, Trial 1

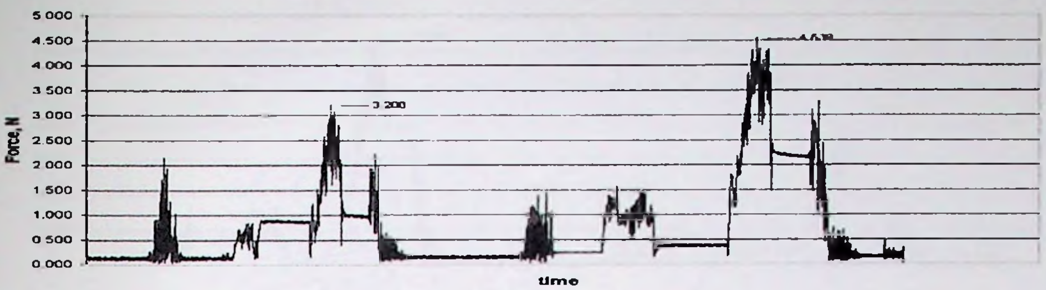

Soil Failure Force, F = 5.2 N
Data code 350102: Soil type 3, alpha =50 deg, H = 10mm, L = 100mm, Trial 2

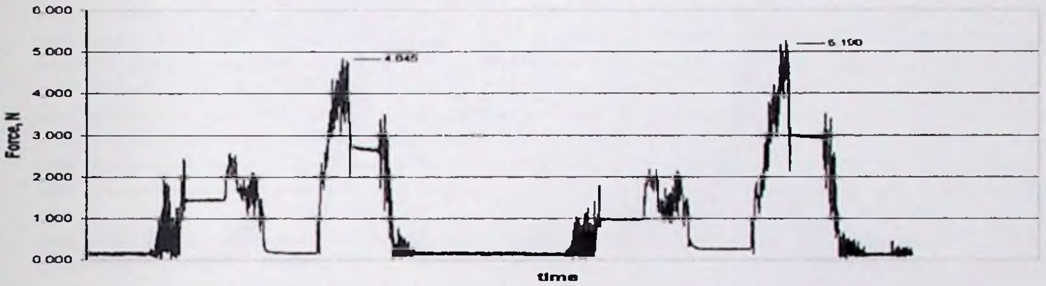

Soil Filure Force, F = 10.46 N
Data code 350201: Soil type 3, alpha =50 deg, H = 20mm, L = 100mm, Trial 1

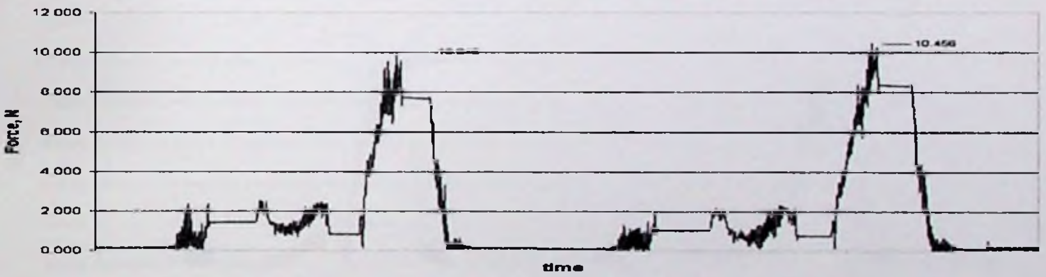

Soil Failure Force, F = 10.63 N
Data code 350202: Soil type 3, alpha =50 deg, H = 20mm, L = 100mm, Trial 2

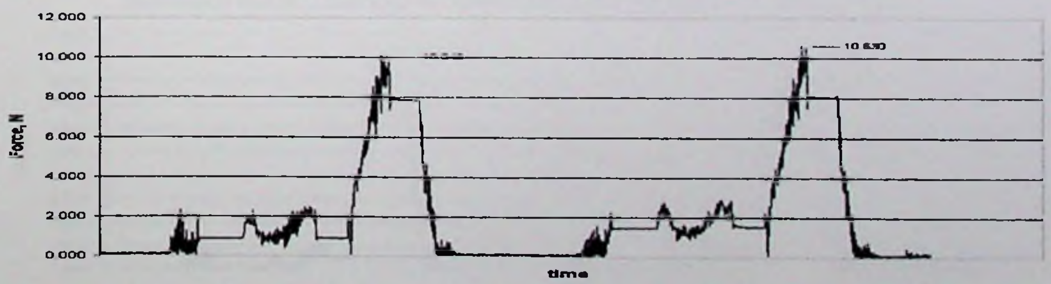

Soil 3 Alpha 60

Soil Failure Force, F = 6.47 N
Data code 360101: Soil type 3, alpha =60 deg, H = 10mm, L = 100mm, Trial 1

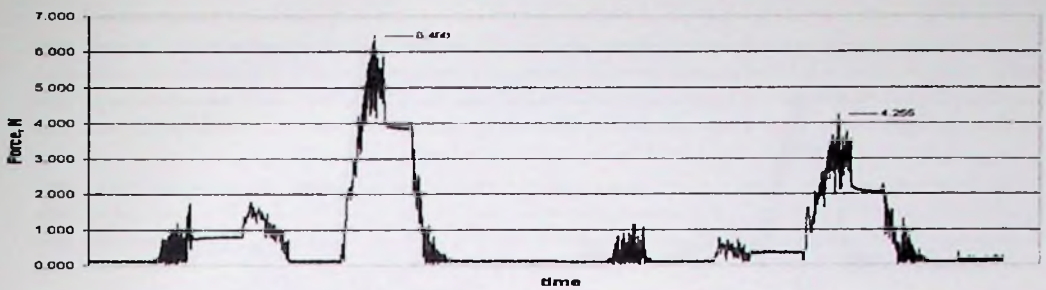

Soil Failure Force, F = 4.61 N
Data code 360102: Soil type 3, alpha =60 deg, H = 10mm, L = 100mm, Trial 2

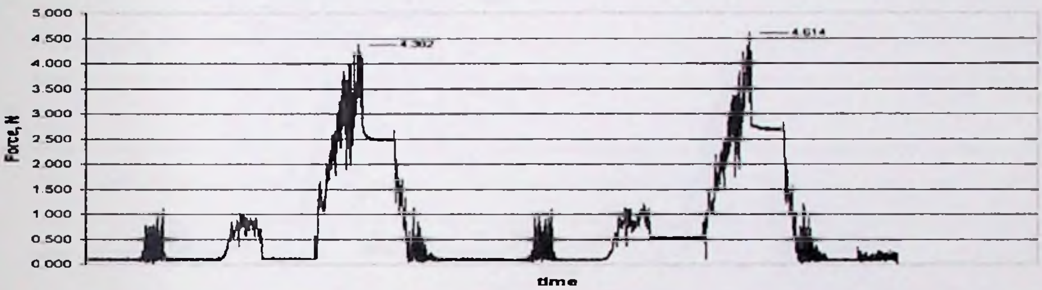

Soil Failure Force, F = 10.15 N
Data code 360201: Soil type 3, alpha =60 deg, H = 20mm, L = 100mm, Trial 1

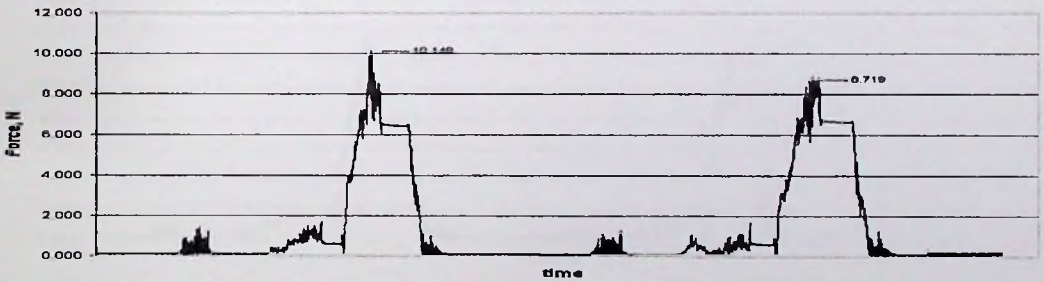

Soil Failure Force, F = 9 N
Data code 360202: Soil type 3, alpha =60 deg, H = 20mm, L = 100mm, Trial 2

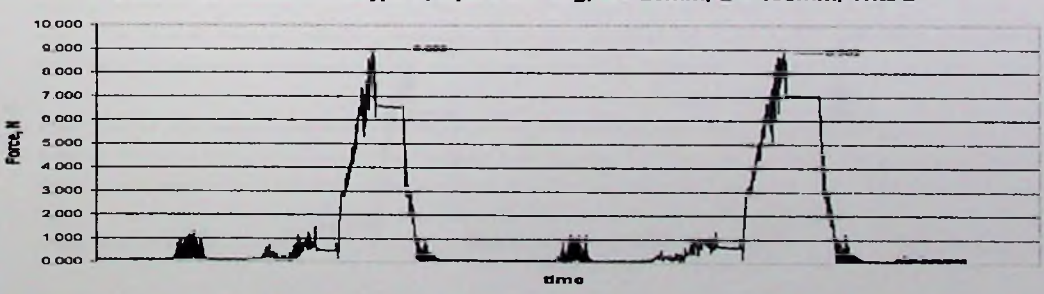

Soil 3 Alpha 70

Soil failure Force, F = 8.26 N
Data code 370101: Soil type 3, alpha =70 deg, H = 10mm, L = 100mm, Trial 1

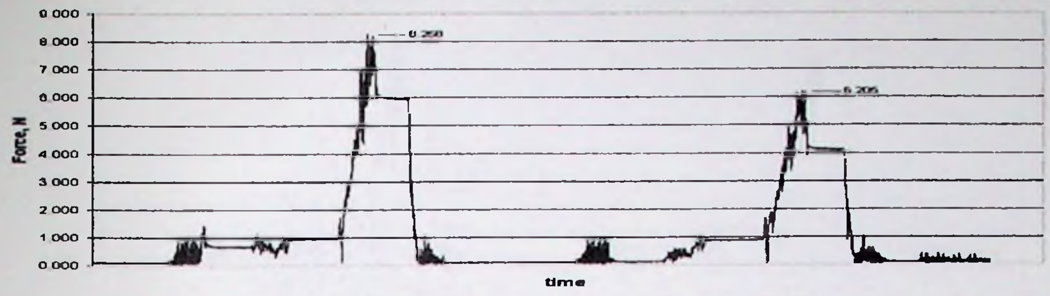

Soil Failure Force, F = 5.78 N
Data code 370102: Soil type 3, alpha =70 deg, H = 10mm, L = 100mm, Trial 2

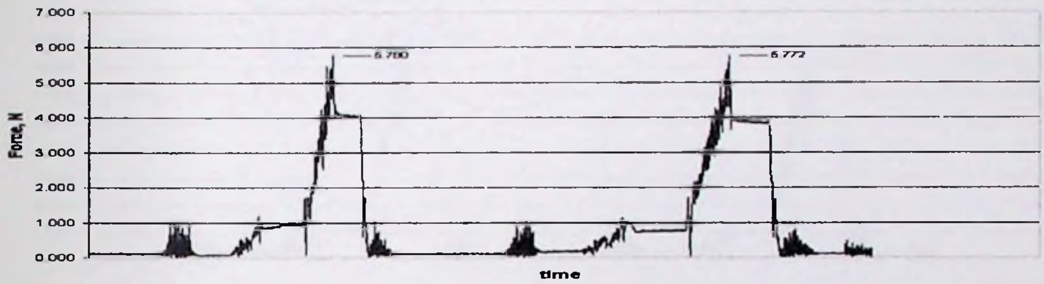

Soil Failure Force, F = 13.96 N
Data code 370201: Soil type 3, alpha =70 deg, H = 20mm, L = 100mm, Trial 1

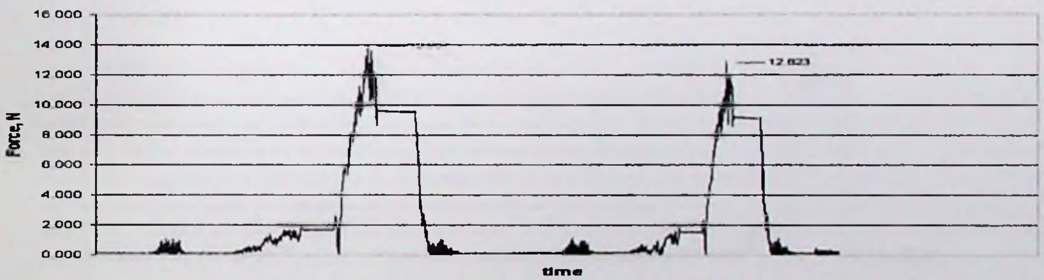

Soil Failure Force, F = 13.25 N
Data code 370202: Soil type 3, alpha =70 deg, H = 20mm, L = 100mm, Trial 2

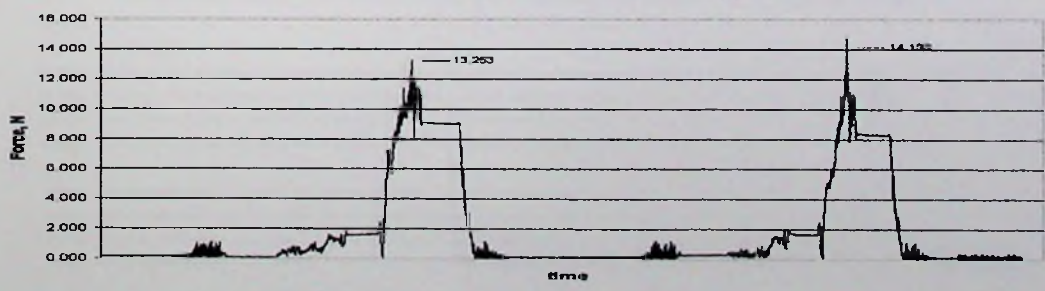

Soil 3 Alpha 80

Soil Failure Force, F = 7.9 N
Data code 380101: Soil type 3, alpha =80 deg, H = 10mm, L = 100mm, Trial 1

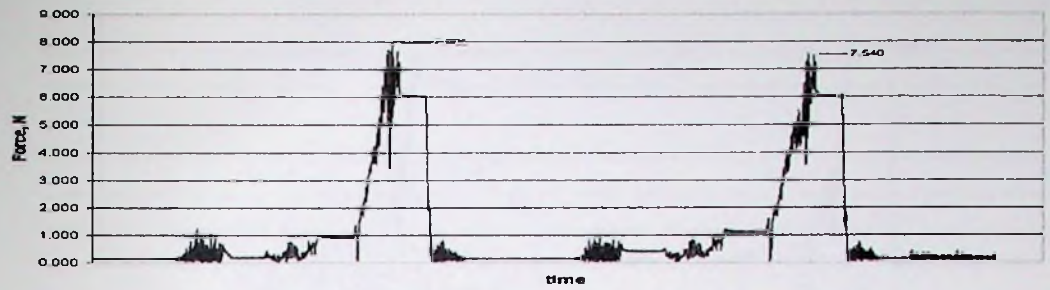

Soil Failure Force, F = 8.1 N
Data code 380102: Soil type 3, alpha =80 deg, H = 10mm, L = 100mm, Trial 2

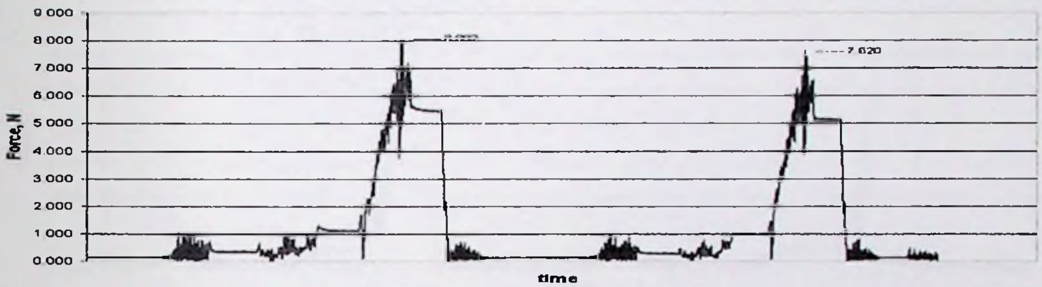

Soil Failure Force, F = 15.46
Data code 380201: Soil type 3, alpha =80 deg, H = 20mm, L = 100mm, Trial 1

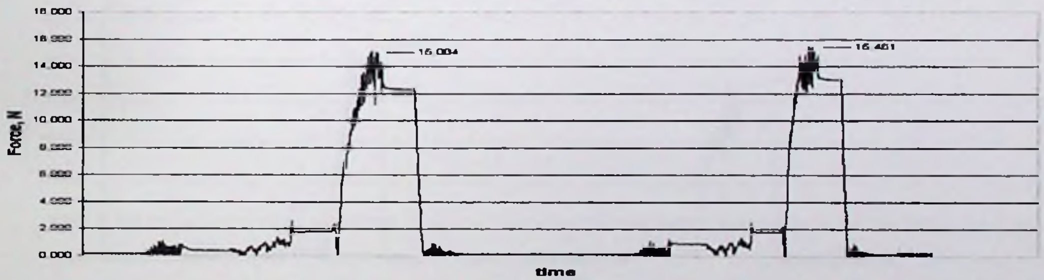

Soil Failure Force, F = 17.33
Data code 380202: Soil type 3, alpha =80 deg, H = 20mm, L = 100mm, Trial 2

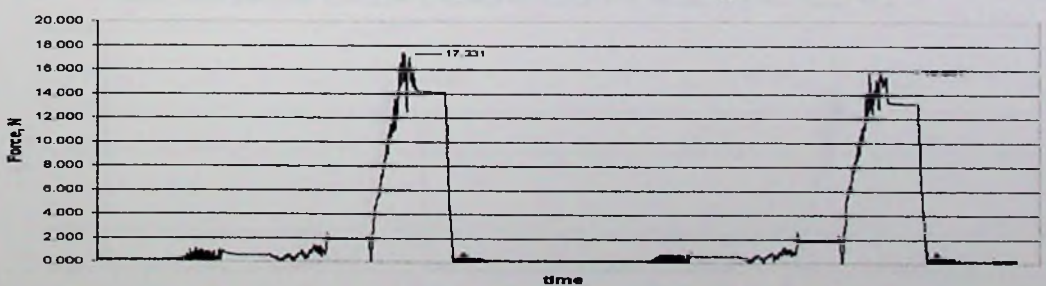

Soil 3 Alpha 90

Soil Failure Force, F = 12.32 N
Data code 390101: Soil type 3, alpha =90 deg, H = 10mm, L = 100mm, Trial 1

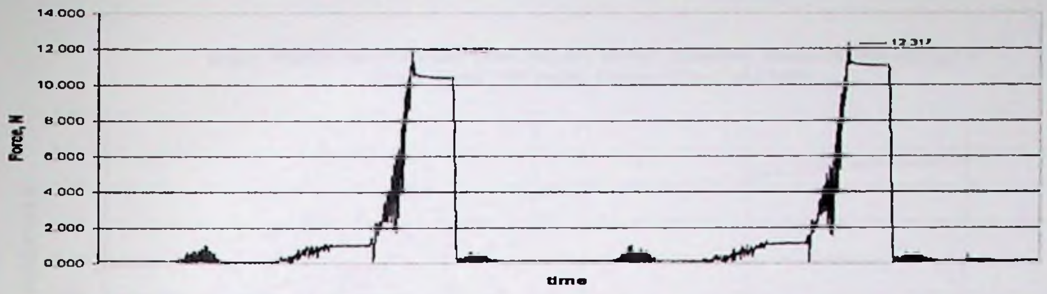

Soil Failure Force, F = 12.2 N
Data code 390102: Soil type 3, alpha =90 deg, H = 10mm, L = 100mm, Trial 2

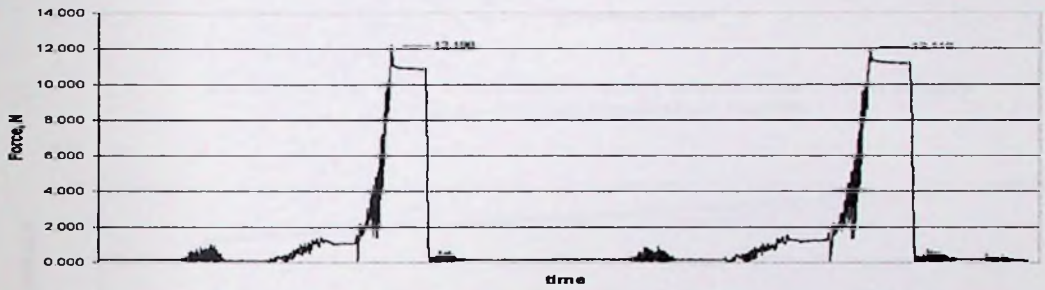

Soil Failure Force, F = 26.84 N
Data code 390201: Soil type 3, alpha =90 deg, H = 20mm, L = 100mm, Trial 1

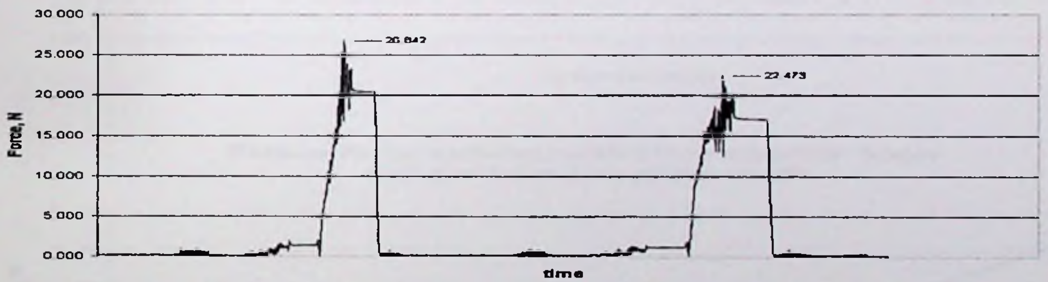

Soil Failure Force, F = 23.88 N
Data code 390202: Soil type 3, alpha =90 deg, H = 20mm, L = 100mm, Trial 2

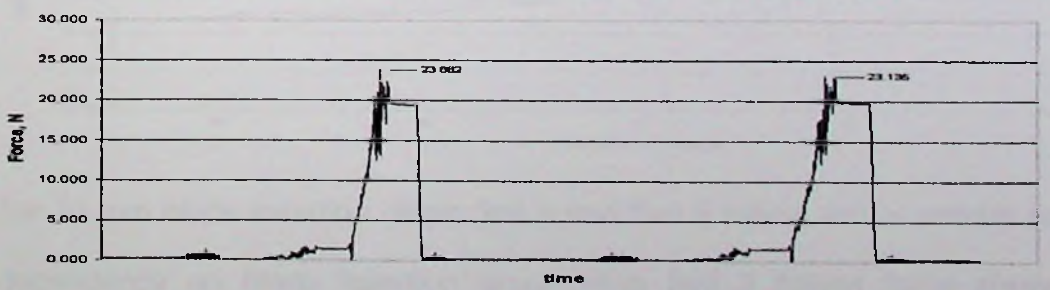

3.3.2 Discussion of soil failure results

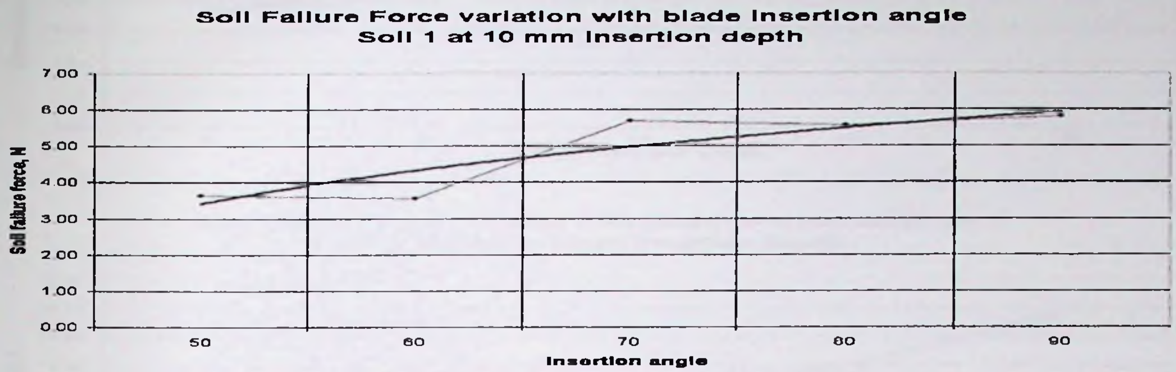

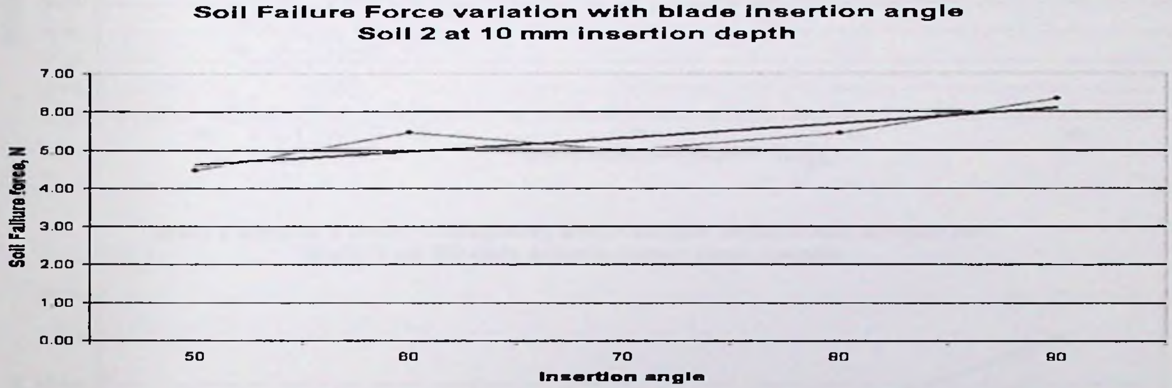

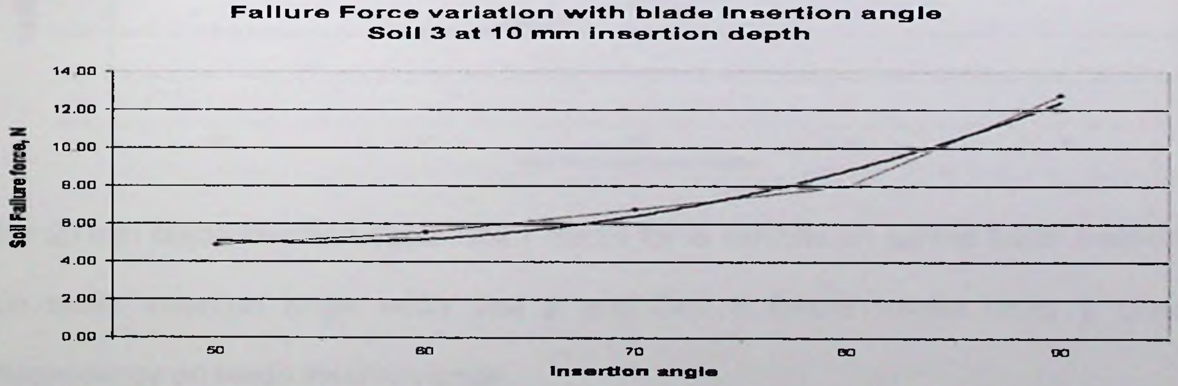

For 10 mm blade insertion depth Soil 1 and Soil 2 failure forces exhibit an almost linear dependency on blade insertion angle while Soil 3 failure force shows a quadratic dependency on blade insertion angle.

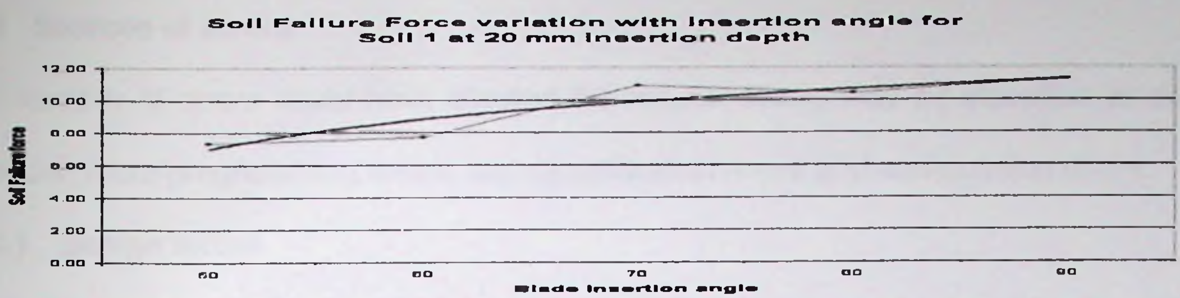

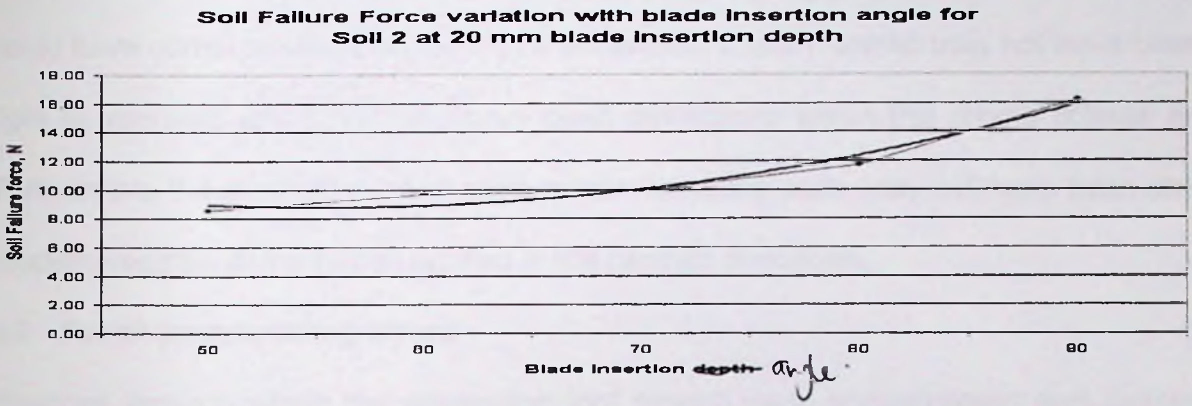

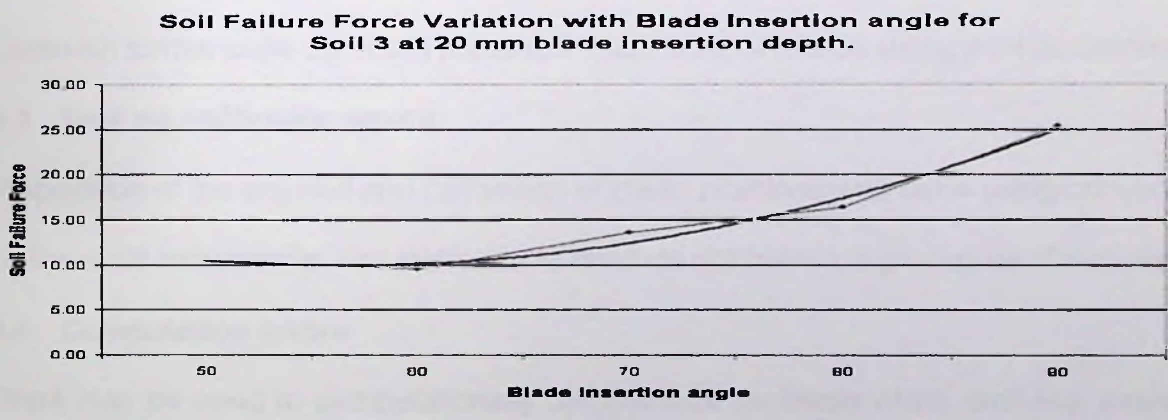

For 20 mm blade insertion depth Soil 1 failure force exhibits an almost linear dependency on blade insertion angle while Soil 2 and Soil 3 failure forces show a quadratic dependency on blade insertion angle.

4 Sources of errors

A number of errors could have affected the results. These may be classified as design errors, robot-programming errors, test rig calibration errors and computation errors.

4.1 Design errors

Using a laboratory scale test rig to obtain results that are representative of field conditions could have compromised accuracy. The excavation blade material may not have been as rigid as required and there may have been deflections within the robots linkage arms. Furthermore the excavation blade and sensor clamping plate may not have been able to properly register all the forces applied in the desired directions.

4.2 Robot-programming errors

Positions through which the excavation tool moved were approximated and defined in Cartesian format while the robot processor must control motion using joint coordinates.

4.3 Test rig calibration errors

Preparation of the soil bed and calibration of blade positions was done using conventional off-the-shelf instruments. The instruments used do not have a high degree of accuracy.

4.4 Computation errors

There may be need to computationally compensate for blade width. Soil tool interaction forces depend highly on surface area of contact between blade and soil. In addition to geometrical factors α, β, **and H,** the amount of soil material being moved also depends on the blade width.

5 Soil property estimation

Using a model developed by [1] and soil failure force data obtained from this project an attempt to estimate soil parameters was made.

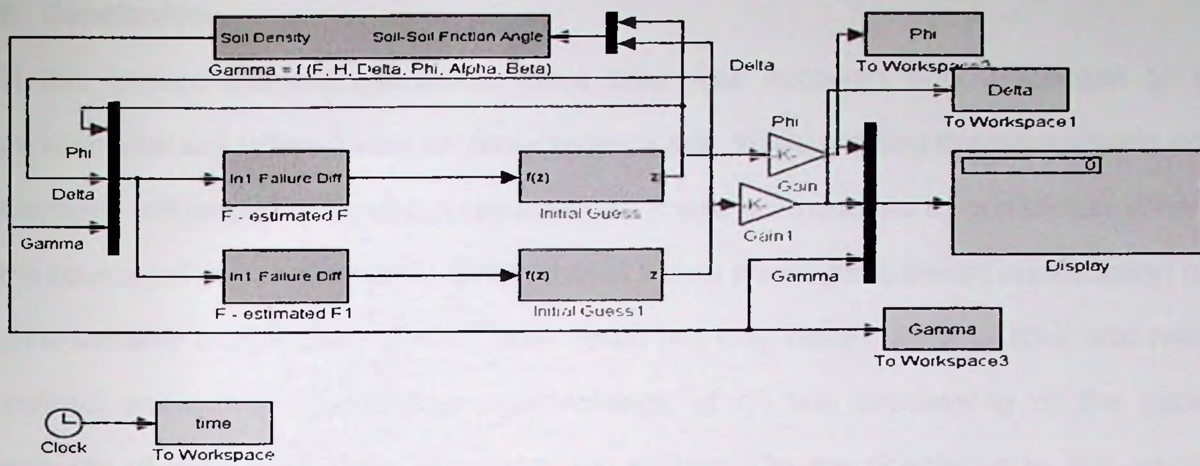

FIGURE 15 MATLAB/SIMULINK MODEL FOR ESTIMATION OF SOIL PARAMETERS

As instructed by **[1]**, soil failure force data for a particular soil and a particular blade insertion angle was fed into the model. Running the MATLAB/Simulink yielded results as shown in figure .

Insertion depth	Soil code	Estimated soil parameters		
		ϕ(degrees)	**δ(degrees)**	**γ (kg/m^3)**
10 mm	1	-34.64	74.56	-2,082
	2	54.64	-42.21	99,100
	3	57.73	-3.86	28,830
20 mm	1	-18.55	74.41	-2,714
	2	224.00	222.50	119,900
	3	-186.40	253.10	15,060

FIGURE 16 RESULTS FROM SOIL PARAMETER ESTIMATION

The above values do not compare well to the experimentally measured values of δ and γ in tables of figures 7 and 11.

6 Conclusion

In this project soil-tool interaction force data was acquired and processed to give experimental soil failure forces for three types of soil. While running the experiments errors inevitably influenced accuracy of results since it was not possible to completely eliminate the sources of errors. Complete elimination of errors would have meant construction of an unnecessarily complicated test rig, that would not only have means of total and reliable external environment sensing but also means of on line processing of the copious amounts of data generated by the sensory system. On the positive side, the ability to embed robot's commands into the MATLAB environment simplified the development of computer programs that control the robot's hand motions. In spite of errors triggered by calibration inaccuracies, programming of tool movements through defined positions was attractive for its simplicity and flexibility. It meant that since it was easy to program, more experiments related to robotic excavation could be run.

The use of soil failure forces from this project's experiments, to estimate soil properties was not successful. This could have been caused by inaccuracies from the sources of errors discussed in chapter 4 or by errors in the soil parameter estimation model used. Therefore soil failure force determination methods used in conjunction with the soil parameter estimation model will need further refinement.

Finally, if these experiments are cost-effectively developed to minimise sources of errors, they are useful in the development of on line soil property estimation for excavation machines for they enhance implementation of intelligent algorithms for automated excavation systems

7 References

[1] C.P Tan, Y.H Zweiri, K. Althoefer & L.D Seneviratne; On-line Soil Property Estimation for Autonomous Excavator Vehicles; *Dept of Mechanical Engineering, King's College London,* EM/2002/06 September 2002

[2] Sanjiv Singh, The State of the Art in Automation of Earthmoving, *ASCE Journal of Aerospace Engineering*, Vol 10, # 4, October 1997

[3] Won Hong, Modeling, Estimation, and Control of Robot-Soil Interactions *Massachusetts institute of technology-Artificial Intelligence Laboratory* AI Technical Report 2001-007, September 2001

[4] Andrew Bond, Force sensing in a Robotic Excavator, *Kings College London B Eng, Mechatronics* Final Year Project report, Appendix 7, May 2002

[5] Alekseeva, T. V. and Artem'ev, K. A. and Bromberg, A. A. and Voitsekhovskii,R. I. and Ul'yanov, N.A., *Machines for Earthmoving Work, Theory and Calculations,*.

[6] [Bernold 86] Bernold, L. E., Low Level Artificial Intelligence and Computer Simulation toPlan and Control Earthmoving Operations. In *Proc. ASCE Speciality conference on Earthmoving and Heavy Equipment*. Tempe, AZ, 1986.

[7] E. Bisse, A. Hemami and E. K. Boukas, A comparison of the required energy in loading for four scooping strategies. In *Proc. 3th International Symposium onMine Mechanization and Automation*, Golden Colorado., Golden, ColoradoUSA, 1995.

[8] [Everett 95] Everett, H. R., *Sensors for Mobile Robots: Theory and Application*, A. K. Peters, Ltd, Wellselly, Massachusetts, 1995 [Feng 92] Feng, P. and Yang, Y. and Qi, Z. and Sun, S., Research on Control Method of

[9] Planning Level for Excavation Robot. In *Proc. 9th International Symposium on Automation and Robotics in Construction.* Tokyo, 1992.

[10] [Hemami 94] H. Hemami. Modeling, analysis, and preliminary studies for automatic scooping, *Advanced Robotics*, pages 1--19, 1994.

8 APPENDICES

8.1 Mitsubishi Move master RV-M1 Micro Robot

- Mitsubishi, RV-M1 (Movemaster EX)
- general purpose commercial arm
- 5 DOF

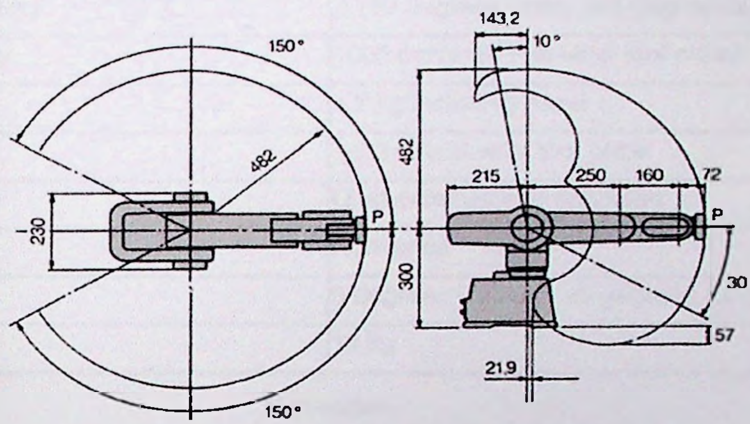

Horizontal work space, in relation to the wrist tool plate.

Vertical work space, in relation to the wrist tool plate.

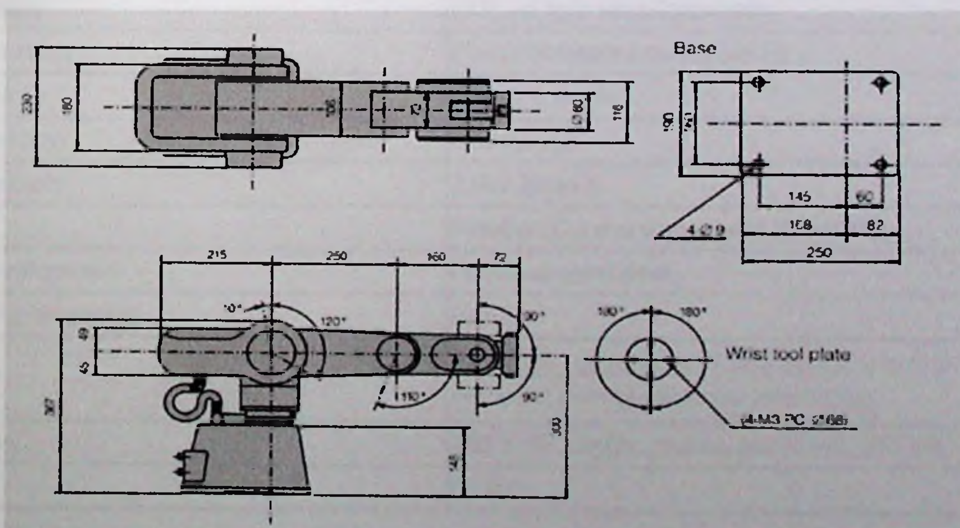

Robot Arm specifications		
Construction		Vertically articulated
Degrees of freedom		5 (not including hand)
Electrical drive system		DC servo motors
Reach		250 + 160 mm
Operation Range	Waist rotation	300 degrees (max. 120 degrees/s)
	Shoulder rotation	130 degrees (max. 72 degrees/s)
	Elbow rotation	110 degrees (max. 109 degrees/s)
	Wrist pitch	±90 degrees (max. 100 degrees/s)
	Wrist roll	±180 degrees (max. 163 degrees/s)
Maximum path velocity		1000 mm/s (PTP at wrist tool plate)
Lifting capacity		1.2 kg including hand
Position repeatability		±0.3 mm at wrist tool plate
Position direction		Limit switches and encoders
Installation position		Horizontal
Ambient temperature		5 degrees Celsius - 40 degrees Celsius
Weight		19 kg

Controller	
Teaching methods	MDI (manual data input) and playback
Control system	PTP, all axis simultaneously
Position detection	Photo detectors and encoders
Speed levels	0 - 9 (10 levels)
Position memory	629 (max.)
Program memory	2,048 (max.)
Interfaces	Parallel (Centronics), serial (RS-232C)
Program development	Personal computer
Programming language	BASIC
External I/O	16 inputs, 16 outputs, EMERGENCY STOP (3 inputs configurable for interrupts)
Power supply	120 V AC, single phase, 50/60 Hz, 500 VA
Weight	23 kg

Source: Industrial micro-robot system/ Model RV-M1 Instruction manual

8.2 Sample MATLAB code

```
function ALPHA25010;
%open and configure serial port RS-232
h=cportopen('com1')
con=cportconfig(h, 'baudrate', 9600, 'stopbits', 2,'parity',1 ,'Bytesize', 7)
%Set hand grip to closed state
%w=cportwrite(h,'SP 1','CR');pause;
%w=cportwrite(h,'GC','CR');pause;
%w=cportwrite(h,'GF 1','CR');pause;
w=cportwrite(h,'NT', 'CR');pause;

%Robot arm positions during the excavation process
%Define positions for a setting of 10mm insertion depth & 50 deg insertion angle
%(0, 400, 235, -45, -6);    Just above soil surface
%(0, 408.4, 225, -45, -6);  Insertion Depth 10mm, ALPHA = 90-(-45 + 85)= 50
%(0, 500, 225, -45, -6);    Horizontal stroke approximately 100mm angle zero
%(0, 400, 360, -45, -6);    Blade extraction stroke

%Set operating speed
w=cportwrite(h,'SP 5','CR');pause(1);       %Set orienting speed
%Start excavation
w=cportwrite(h,'MP 0, 400, 360, -45, -6', 'CR');pause;
w=cportwrite(h,'SP 9','CR');pause(0.5);     %Set positioning speed
w=cportwrite(h,'MP 0, 400, 240, -45, -6', 'CR');pause(2);
w=cportwrite(h,'SP 2','CR');pause(0.5);     %Set blade insertion speed
w=cportwrite(h,'MP 0, 408.4, 230, -45, -6', 'CR');pause(2.5);
w=cportwrite(h,'SP 9','CR');pause(0.5);     %Set horizontal stroke speed
w=cportwrite(h,'MP 0, 500, 230, -45, -6', 'CR');pause(2);
w=cportwrite(h,'MP 0, 400, 360, -45, -6', 'CR');pause;   %Pause to prepare soils
for next excavation
%Repeat excavation cycle
w=cportwrite(h,'MP 0, 400, 240, -45, -6', 'CR');pause(2);
w=cportwrite(h,'SP 2','CR');pause(0.5);     %Set blade insertion speed
w=cportwrite(h,'MP 0, 408.4, 230, -45, -6', 'CR');pause(2.5);
w=cportwrite(h,'SP 9','CR');pause(0.5);     %Set horizontal stroke speed
w=cportwrite(h,'MP 0, 500, 230, -45, -6', 'CR');pause(2);
w=cportwrite(h,'MP 0, 400, 360, -45, -6', 'CR');pause(2);
%Return to nest position
w=cportwrite(h,'NT', 'CR');
f=cportclose(h)
```

```
function ALPHA25020;
%open and configure serial port RS-232
h=cportopen('com1')
con=cportconfig(h, 'baudrate', 9600, 'stopbits', 2,'parity',1 ,'Bytesize', 7)
%Set hand grip to closed state
%w=cportwrite(h,'SP 1','CR');pause;
%w=cportwrite(h,'GC','CR');pause;
%w=cportwrite(h,'GF 1','CR');pause;
w=cportwrite(h,'NT', 'CR');pause;

%Robot arm positions during the excavation process
%Define positions for a setting of 20mm insertion depth & 50 deg insertion angle
%(0, 400, 235, -45, -6);    Just above soil surface
%(0, 416.8, 215, -45, -6);  Insertion Depth 20mm, ALPHA = 90-(-45 + 85)= 50
%(0, 500, 215, -45, -6);    Horizontal stroke approximately 100mm
%(0, 400, 360, -45, -6);    Blade extraction stroke

%Set operating speed
w=cportwrite(h,'SP 5','CR');pause(1);       %Set orienting speed
%Start excavation
w=cportwrite(h,'MP 0, 400, 360, -45, -6', 'CR');pause;
w=cportwrite(h,'SP 9','CR');pause(0.5);     %Set positioning speed
w=cportwrite(h,'MP 0, 400, 240, -45, -6', 'CR');pause(2);
w=cportwrite(h,'SP 2','CR');pause(0.5);     %Set blade insertion speed
w=cportwrite(h,'MP 0, 416.8, 220, -45, -6', 'CR');pause(2.5);
w=cportwrite(h,'SP 9','CR');pause(0.5);     %Set horizontal stroke speed
w=cportwrite(h,'MP 0, 500, 220, -45, -6', 'CR');pause(2);
w=cportwrite(h,'MP 0, 400, 360, -45, -6', 'CR');pause;   %Pause to prepare soils
for next excavation
%Repeat excavation cycle
w=cportwrite(h,'MP 0, 400, 240, -45, -6', 'CR');pause(2);
w=cportwrite(h,'SP 2','CR');pause(0.5);     %Set blade insertion speed
w=cportwrite(h,'MP 0, 416.8, 220, -45, -6', 'CR');pause(2.5);
w=cportwrite(h,'SP 9','CR');pause(0.5);     %Set horizontal stroke speed
w=cportwrite(h,'MP 0, 500, 220, -45, -6', 'CR');pause(2);
w=cportwrite(h,'MP 0, 400, 360, -45, -6', 'CR');pause(2);
%Return to nest position
w=cportwrite(h,'NT', 'CR');
f=cportclose(h)
```

```
function ALPHA39010;
%open and configure serial port RS-232
h=cportopen('com1')
con=cportconfig(h, 'baudrate', 9600, 'stopbits', 2,'parity',1 ,'Bytesize', 7)
%Set hand grip to closed state
%w=cportwrite(h,'SP 1','CR');pause;
%w=cportwrite(h,'GC','CR');pause;
%w=cportwrite(h,'GF 1','CR');pause;
w=cportwrite(h,'NT', 'CR');pause;

%Robot arm positions during the excavation process
%Define positions for a setting of 10mm & 90 deg insertion depth & angle
respectively
%(0, 300, 240, -85, -6', 'CR');     Just above soil surface
%(0, 300, 230, -85, -6', 'CR');     Insertion Depth 20mm, ALPHA = 90-(-85 + 85)=
90
%(0, 400, 230, -85, -6', 'CR');     Horizontal stroke 100mm angle zero
%(0, 250, 360, -85, -6', 'CR');     Blade extraction stroke

%Set operating speed
w=cportwrite(h,'SP 5','CR');pause(1);       %Set orienting speed
%Start excavation
w=cportwrite(h,'MP 0, 250, 360, -85, -6', 'CR');pause;
w=cportwrite(h,'SP 9','CR');pause(0.5);     %Set positioning speed
w=cportwrite(h,'MP 0, 300, 245, -85, -6', 'CR');pause(2);
w=cportwrite(h,'SP 2','CR');pause(0.5);     %Set blade insertion speed
w=cportwrite(h,'MP 0, 300, 235, -85, -6', 'CR');pause(2);
w=cportwrite(h,'SP 9','CR');pause(0.5);     %Set horizontal stroke speed
w=cportwrite(h,'MP 0, 400, 235, -85, -6', 'CR');pause(2);
w=cportwrite(h,'MP 0, 250, 360, -85, -6', 'CR');pause;       %Pause to prepare
soils for next excavation
%Repeat excavation cycle
w=cportwrite(h,'MP 0, 300, 245, -85, -6', 'CR');pause(2);
w=cportwrite(h,'SP 2','CR');pause(0.5);     %Set blade insertion speed
w=cportwrite(h,'MP 0, 300, 235, -85, -6', 'CR');pause(2);
w=cportwrite(h,'SP 9','CR');pause(0.5);     %Set horizontal stroke speed
w=cportwrite(h,'MP 0, 400, 235, -85, -6', 'CR');pause(2);
w=cportwrite(h,'MP 0, 250, 360, -85, -6', 'CR');pause(2);
%Return to nest position
w=cportwrite(h,'NT', 'CR');
f=cportclose(h)
```

```
function ALPHA39020;
%open and configure serial port RS-232
h=cportopen('com1')
con=cportconfig(h, 'baudrate', 9600, 'stopbits', 2,'parity',1 ,'Bytesize', 7)
%Set hand grip to closed state
%w=cportwrite(h,'SP 1','CR');pause;
%w=cportwrite(h,'GC','CR');pause;
%w=cportwrite(h,'GF 1','CR');pause;
w=cportwrite(h,'NT', 'CR');pause;

%Robot arm positions during the excavation process
%Define positions for a setting of 20mm & 0 deg insertion depth & angle
respectively
%(0, 300, 240, -85, -6', 'CR');     Just above soil surface
%(0, 300, 220, -85, -6', 'CR');     Insertion Depth 20mm, ALPHA = 90-(-85 + 85)=
90
%(0, 400, 220, -85, -6', 'CR');     Horizontal stroke 100mm
%(0, 250, 360, -85, -6', 'CR');     Blade extraction stroke

%Set operating speed
w=cportwrite(h,'SP 5','CR');pause(1);       %Set orienting speed
%Start excavation
w=cportwrite(h,'MP 0, 250, 360, -85, -6', 'CR');pause;
w=cportwrite(h,'SP 9','CR');pause(0.5);     %Set positioning speed
w=cportwrite(h,'MP 0, 300, 245, -85, -6', 'CR');pause(2);
w=cportwrite(h,'SP 2','CR');pause(0.5);     %Set blade insertion speed
w=cportwrite(h,'MP 0, 300, 225, -85, -6', 'CR');pause(2);
w=cportwrite(h,'SP 9','CR');pause(0.5);     %Set horizontal stroke speed
w=cportwrite(h,'MP 0, 400, 225, -85, -6', 'CR');pause(2);
w=cportwrite(h,'MP 0, 250, 360, -85, -6', 'CR');pause;       %Pause to prepare
soils for next excavation
%Repeat excavation cycle
w=cportwrite(h,'MP 0, 300, 245, -85, -6', 'CR');pause(2);
w=cportwrite(h,'SP 2','CR');pause(0.5);     %Set blade insertion speed
w=cportwrite(h,'MP 0, 300, 225, -85, -6', 'CR');pause(2);
w=cportwrite(h,'SP 9','CR');pause(0.5);     %Set horizontal stroke speed
w=cportwrite(h,'MP 0, 400, 225, -85, -6', 'CR');pause(2);
w=cportwrite(h,'MP 0, 250, 360, -85, -6', 'CR');pause(2);
%Return to nest position
w=cportwrite(h,'NT', 'CR');
f=cportclose(h)
```

8.3 Trolley and Sand box design

8.3.1 Plan, side and elevation view of trolley design

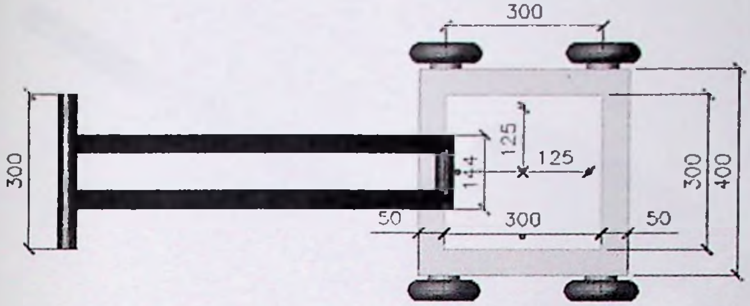

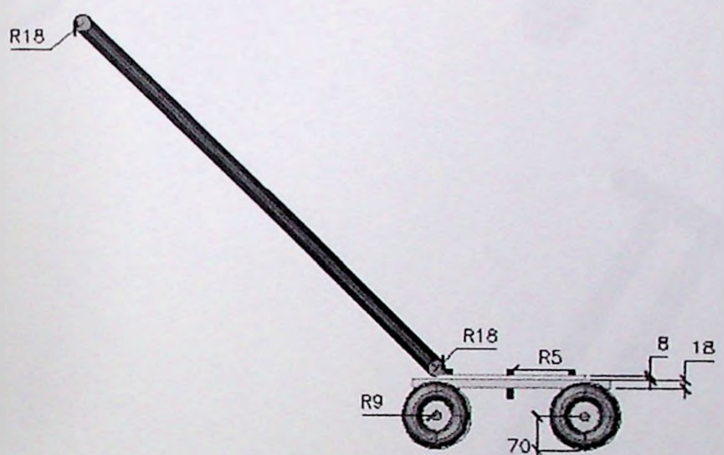

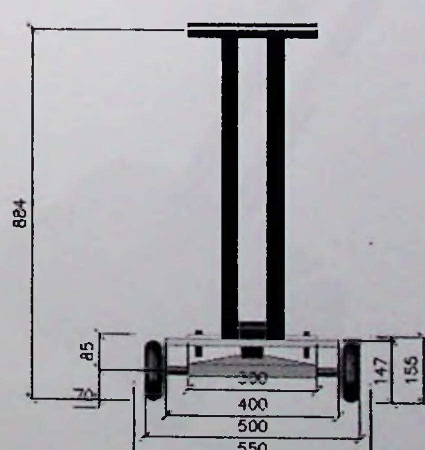

8.3.2 Perspective views of trolley design

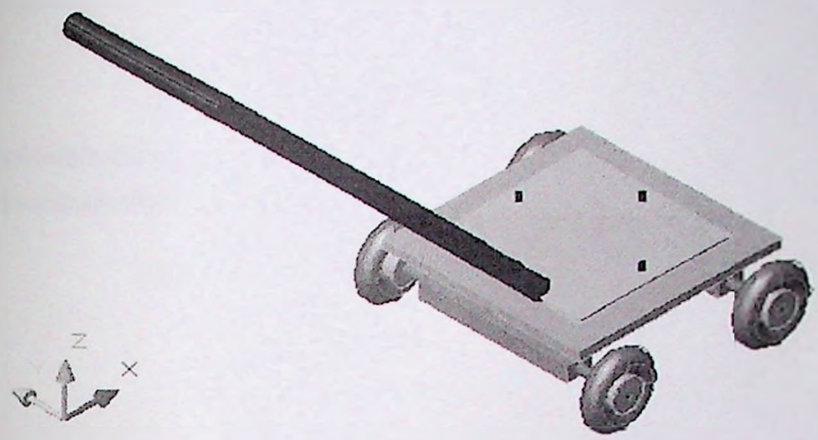

8.3.3 Plan, side and elevation views of the test rig platform design

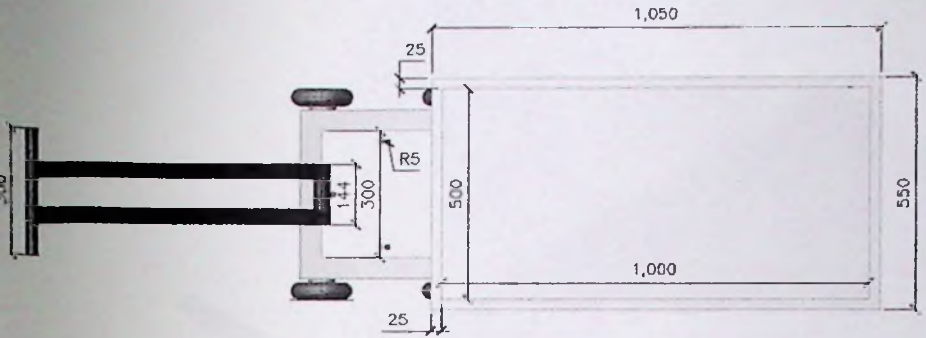

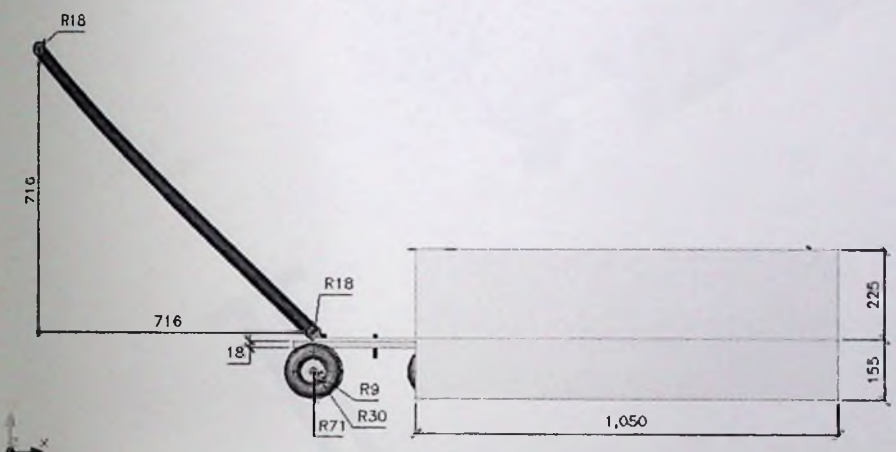

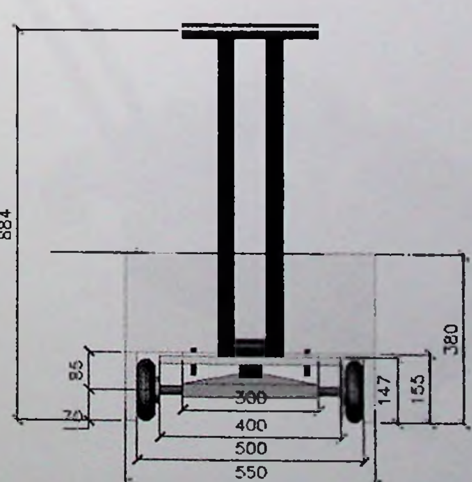

8.3.4 Perspective views of the test rig platform design

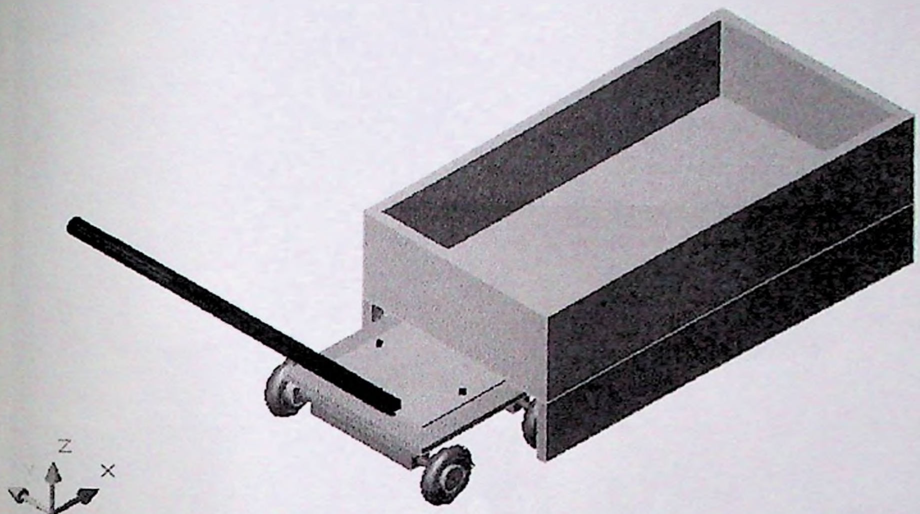

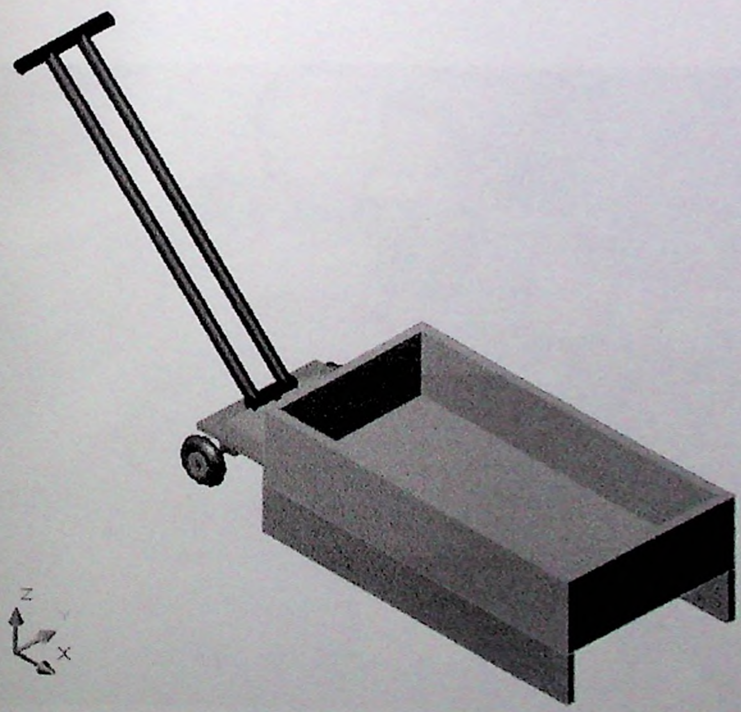

8.4 Test rig photos

8.4.1 90° orientation

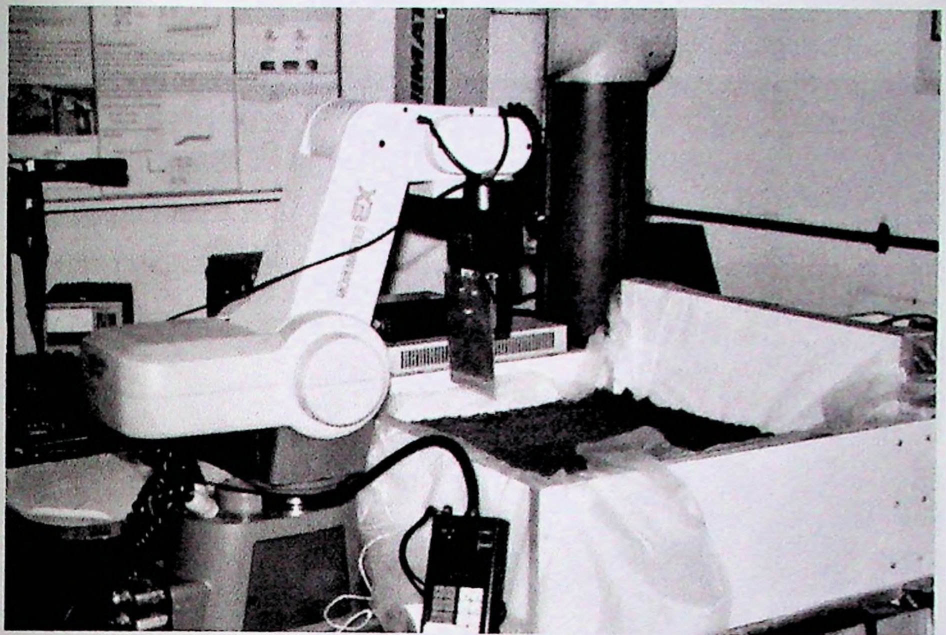

B.4.2 60° Orientation

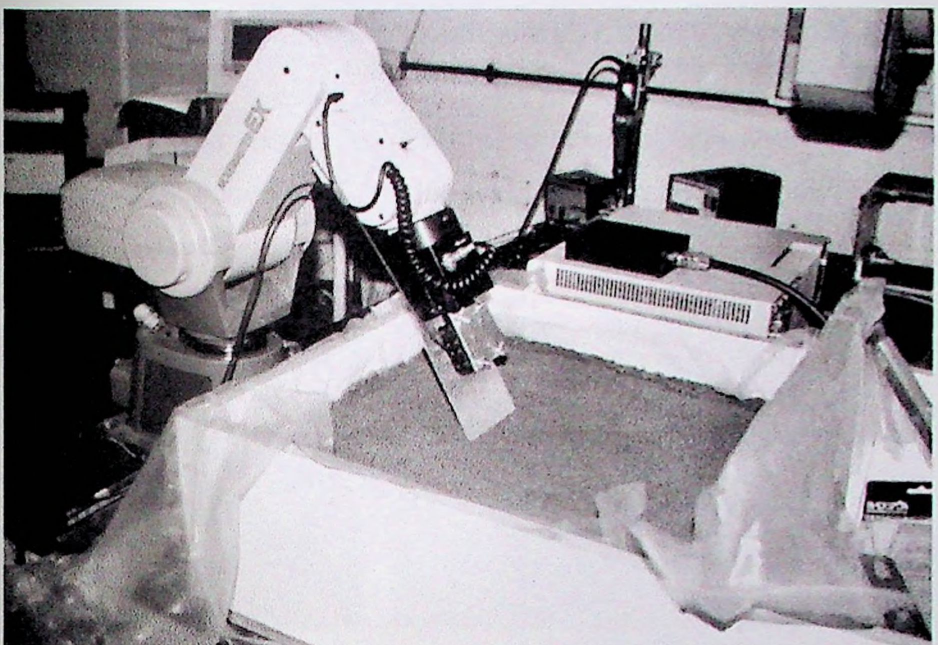

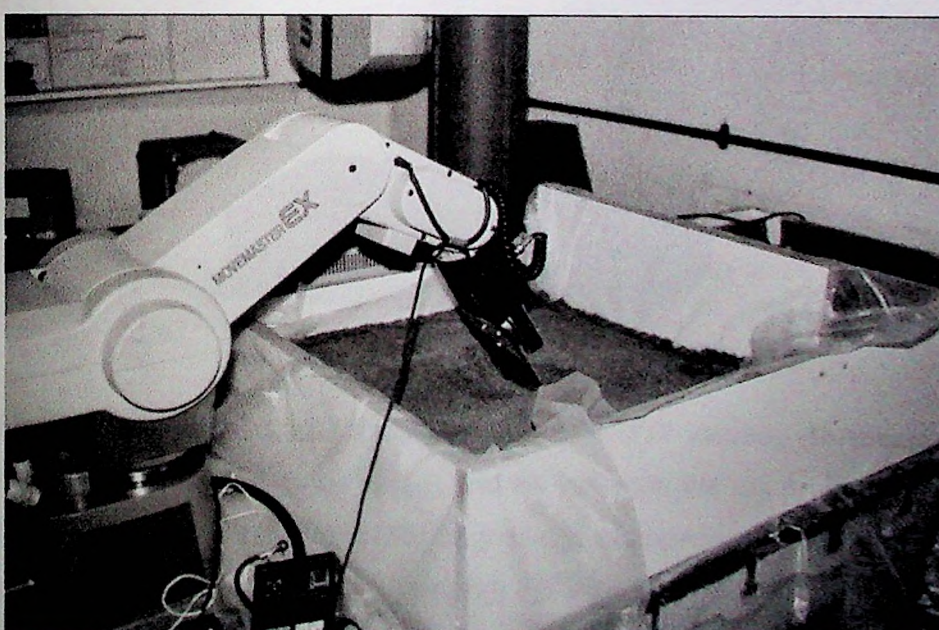

8.5 Sensor description and specifications

Measures 6-axis forces and torques (Fx, Fy, Fz, Tx, Ty, Tz)

The F/T sensor system measures all six components of force and torque. It consists of a transducer, shielded high-flex cable, and intelligent ISA or stand-alone controller.

Transducer

The compact and rugged monolithic transducer uses silicon strain gauges to sense forces. The transducer's silicon strain gauges provide high noise immunity and allow high overload protection, which is standard on all models.

Controller F/T

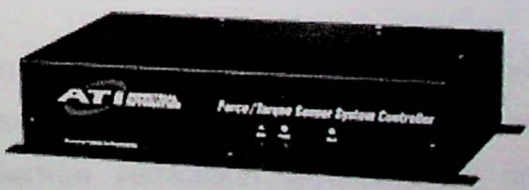

The stand-alone controller outputs forces and torques (F/T values) via the standard RS-232 serial port at a variety of baud rates, and as voltages via an analogue port. Digital discrete I/O capability is available for signalling user-programmed F/T thresholds, monitoring system health, and biasing (zeroing) F/T values.

Built-in Capabilities

Both the DAQ F/T and Controller F/T provide a variety of powerful functions:

- **Tool transformations** translate and/or rotate the F/T reference frame.
- **Demo software allows simple data logging routines**
- **Biasing** provides a convenient way to offset tool weight.
- **Increased system throughput** is possible by reducing the number of axes output.
- **Temperature compensation** option insures accuracy over a wide temperature range.

Key Features and Benefits

- **Overload protection:** The F/T transducer is extremely rugged and durable. All transducer models can withstand high overload.
- **High signal-to-noise ratio:** Silicon gages provide a signal 75 times stronger than conventional foil gages. This signal is amplified resulting in near-zero noise distortion.
- **High-speed output** of over 7800 Hz with ISA controller exceeds requirements for most applications.
- **Prompt delivery** of standard F/T models.
- **Custom F/T sensors** can be designed and built to your specifications.
- **Application assistance** by experienced engineers.

Applications

ATI Industrial Automation is the largest supplier of 6-axis force/torque sensors in the world. Thousands of F/T sensors are being used in a variety of applications such as:

- **Robotic part insertion** verification of mechanical and electrical component assembly.
- **Deburring, polishing, grinding** where robot is required to apply a constant force.
- **Force/torque feedback** for manipulators in nuclear environments.
- **Physical rehabilitation** and prosthetics research.
- **Product testing** - such as steering wheel torque and automotive seat testing.

Standard Calibrations

Transducer	English	Metric
Nano17	US-3-1	SI-12-0.12
	US-6-2	SI-25-0.25
Nano 25	US-25-25	SI-125-3
	US-50-50	SI-250-6
Nano 43	US-4-2	SI-18-0.25
	US-8-4	SI-36-0.5
Mini 40	US-5-10	SI-20-1
	US-10-20	SI-40-2
Mini 45	US-30-40	SI-145-5
	US-60-80	SI-290-10
Gamma	US-7.5-25	SI-32-2.5
	US-15-50	SI-65-5
Delta	US-75-300	SI-330-30
	US-150-600	SI-660-60
Theta	US-200-1000	SI-1000-120
	US-350-2100	SI-1500-240
Omega160	US-200-1000	SI-1000-120
	US-350-2100	SI-1500-240
Omega190	US-400-3000	SI-1800-350
	US-800-6000	SI-3600-700

Maximum Single-Axis Load

Transducer Body	Axes	English	Metric
Nano17	Fxy	± 79 lbs	± 350 N
	Fz	± 180 lbs	± 800 N
	Txy	± 23 in-lbs	± 2.6 N-m
	Tz	± 28 in-lbs	± 3.1 N-m
Nano25	Fxy	± 520 lbs	± 2325 N
	Fz	± 1400 lbs	± 6250 N
	Txy	± 310 in-lbs	± 34 N-m
	Tz	± 560 in-lbs	± 62 N-m
Nano 43	Fxy	± 68 lbs	± 300 N
	Fz	± 89 lbs	± 400 N
	Txy	± 30 in-lbs	± 3.4 N-m
	Tz	± 48 in-lbs	± 5.4 N-m
Mini40	Fxy	± 200 lbs	± 870 N
	Fz	± 610 lbs	± 2700 N
	Txy	± 190 in-lbs	± 21 N-m
	Tz	± 190 in-lbs	± 21 N-m
Mini 45	Fxy	± 1200 lbs	± 5100 N
	Fz	± 2300 lbs	± 10000 N
	Txy	± 950 in-lbs	± 110 N-m
	Tz	±1200 in-lbs	± 140 N-m
Gamma	Fxy	± 270 lbs	± 1200 N
	Fz	± 910 lbs	± 4100 N
	Txy	± 690 in-lbs	± 79 N-m
	Tz	± 730 in-lbs	± 82 N-m
Delta	Fxy	± 770 lbs	± 3400 N
	Fz	± 2600 lbs	± 12000 N
	Txy	± 2000 in-lbs	± 220 N-m
	Tz	± 3700 in-lbs	± 420 N-m
Theta	Fxy	± 5700 lbs	± 25000 N
	Fz	± 14000 lbs	± 61000 N
	Txy	± 22000 in-lbs	± 2500 N-m
	Tz	± 24700 in-lbs	± 2700 N-m
Omega 160	Fxy	± 4000 lbs	±18000 N
	Fz	±11000 lbs	± 48000 N
	Txy	±15000 in-lbs	±1700 N-m
	Tz	±17000 in-lbs	±1900 N-m
Omega190	Fxy	± 8000 lbs	± 36000 N
	Fz	± 25000 lbs	±11000 N
	Txy	± 49000 in-lbs	± 5500 N-m
	Tz	± 72000 in-lbs	± 8100 N-m

Additional Options

- Dual-gain option: It is possible to have two calibrations with one F/T model. A manually operated switch allows you to select transducer gain setting; you must also instruct the controller to change from one calibration to another. You can use the F/T with a low payload and a high resolution, then switch to a higher payload calibration with a lower resolution.
- Temperature compensation option: The F/T has an approximate gain shift error of 0.1% degree F from the calibration temperature. The temperature compensation will correct for this gain shift error, proving a more accurate sensor.

Source: ATI-Industrial Automation [www.ati-ia.com]